NASA CONTRACTOR REPORT

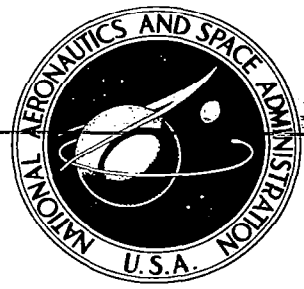

NASA CR-861

STUDY OF CERAMIC HEAT SHIELDS FOR LIFTING REENTRY VEHICLES

by J. N. Krusos

Prepared by
BELL AEROSYSTEMS COMPANY
Buffalo, N. Y.
for Langley Research Center

NATIONAL AERONAUTICS AND SPACE ADMINISTRATION • WASHINGTON, D. C. • AUGUST 1967

NASA CR-861

STUDY OF CERAMIC HEAT SHIELDS FOR LIFTING REENTRY VEHICLES

By J. N. Krusos

Prepared under Contract No. NAS 1-5370 by
BELL AEROSYSTEMS COMPANY
Buffalo, N.Y.

for Langley Research Center

NATIONAL AERONAUTICS AND SPACE ADMINISTRATION

For sale by the Clearinghouse for Federal Scientific and Technical Information
Springfield, Virginia 22151 – CFSTI price $3.00

FOREWORD

This report was prepared by Bell Aerosystems Company under NASA Contract NAS 1-5370 and covers the work performed during the period August 1965 to October 1966. The contract was administered under the direction of Mr. Donald R. Rummler, Contracting Officer's Representative, and Mr. John G. Davis, Jr., Alternate Contracting Officer's Representative, at NASA, Langley Research Center.

The author wishes to acknowledge the contributions of the following Bell Aerosystems personnel:

John T. Witmer	-	Design Concept Studies
Roger G. Higgins	-	Structural Design
Rolland D. Huff	-	Thermo-Structural Analysis
Michael S. Janis	-	Heat Transfer Analysis
Leon Marcus and Darwin Marshall	-	Ceramic Technology
James Y. Ho	-	Brittle Material Statistical Studies
Stephan Jordan	-	Dynamics Analysis

TABLE OF CONTENTS

TABLE OF CONTENTS (CONT)

LIST OF ILLUSTRATIONS

LIST OF ILLUSTRATIONS (CONT)

TABLES

SYMBOLS

A	Cross-sectional Area Support Flexibility Factor for Expansion Restraint
A_N	Total Cross-sectional Area
A_r	Cross-sectional Area of Unbroken Fibers
A_S	Shear Area
B	Support Flexibility Factor for Bowing Restraint
d	Material Thickness, Spherical Pore Diameter
E	Modulus of Elasticity
F	Probability of Failure
G	Sublayer of Material
H	Sublayer of Material
h	Heat Transfer Coefficient
k	Thermal Conductivity or Thermal Conductance
L/D	Lift-Drag Ratio
M	Sublayer of Material, Total of All Sublayers
m	Material Variability Constant
N	Number of Sublayers for Each Material, Number of Fibers
n	Material Characteristic
P	Force
p	Volume Fraction Porosity
q	Number of Fibers Broken
q	Cold Wall Heat Flux

SYMBOLS (CONT)

r	Number of Fibers Unbroken, Radius
T_R	Boundary Layer Recovery Temperature
T_{w_o}	Cold Wall Temperature
T_1	Absolute Surface Temperature
ΔT	Temperature Change
V	Volume
X	Rupture Strength Distribution
X_o	Material Characteristic Stress
X_u	Threshold Stress
$(X)_o$	Tensile Stress on Each Fiber When No Fiber Has Been Broken
ΔX	Structural Cross-section Increments
Z'	Distance from Neutral Axis
$\overline{Z}$	Location of Neutral Axis
ΔZ	Thickness of a Sublayer
X,Y,Z	Rectangular Cartesian Coordinates
α	Coefficient of Thermal Expansion
ϵ	Plate Expansion, Strain
$\Delta\theta$	Time Increments
υ	Poisson's Ratio
σ	Thermal Stress
σ_o	Strength
σ_A	Allowable Stress
ω	Curvature (Reciprocal of the Radius of Curvature)

SUBSCRIPTS

bf	Backface
CER, C	Ceramic
if	Interface
L	Lower Boundary
j	Point Within the Plate Thickness
min	Minimum
max	Maximum
S	Surface, Shear
U	Upper Boundary
W	Wire
X,Y	Rectangular Cartesian Coordinates

STUDY OF CERAMIC HEAT SHIELDS FOR LIFTING REENTRY VEHICLES

by

J. N. Krusos

SUMMARY

An analytical and experimental study was conducted to determine and assess radiative ceramic heat shield designs for manned lifting entry vehicles. Porous forms of ceramics were selected to provide advantageous insulation and weight characteristics. Candidate materials and their appropriate porous structure were determined through thermal stress analyses, heat transfer studies, and thermal shock tests which simulated the most severe heating conditions for representative vehicle reentry trajectories. The materials which demonstrated repetitive thermal shock capability were incorporated into heat shield designs. Optimization studies were then applied to define minimum weight shields for the three most promising ceramic materials.

Statistical studies were made to describe approaches for understanding the strength properties of highly porous refractory bodies, their response to mechanical loads, and their apparent marked insensitivity to notches and flaws as compared to dense brittle materials. However, considerable additional analytical and experimental work is required to provide a working knowledge for porous structures.

The state-of-the-art of manufacturing ceramics was reviewed, and recommendations were developed for achieving uniformity and control of quality. Inspection techniques were reviewed in relation to vehicle needs, including repeated flight capability.

The ceramic heat shield concepts were compared with ablative shields with respect to cost, weight, reliability, and other aspects. The ceramic designs were found competitive, though further effort is required to overcome deficiciencies in material and analytical technologies in order to achieve the full potential of refractory radiative shields.

I. INTRODUCTION

To date, heat protection technology for manned reentry vehicles has dealt primarily with blunt aerodynamic shapes with low lift-to-drag characteristics. The time of reentry is short for such vehicles and ablative shields have satisfied heat protection needs. The advent of lift body vehicle concepts, such as the HL-10, with ability to maneuver and land at ground sites, has introduced more difficult heat protection requirements by substantially extending the time period of intense aerodynamic heating during reentry. A number of approaches are available for developing satisfactory heat shields for long reentry flight, including modified ablative designs as well as the use of highly refractory ceramic materials which would provide the desired resistance to the environment. This study examined the application of porous ceramics to heat shield designs and endeavored to assess the potential advantages and problems offered by ceramic materials to the specific heat shield requirements of lift body vehicles.

Basically, the potential advantages of a ceramic heat shield system are as follows:

1. The ability to maintain smooth and stable vehicle contours during reentry in order to facilitate vehicle control and maneuverability.

2. Use of materials physically and chemically stable in the flight environment to permit repeated flight with little or no refurbishment.

3. Lightweight system, since heat protection is based on radiation rejection of a very large proportion of the incident heat.

4. Low heat shield cost attributable to the reusability of ceramic shields.

A number of significant deficiencies have existed in the technology of solid and porous ceramics which have impeded the application of ceramic materials to aerospace structural and heat protection applications. The deficiencies have included: (1) inability to analyze and accurately predict mechanical and thermal stress performance; (2) lack of well defined design and test procedures to establish high reliability for components made of brittle materials; and (3) difficulty in assuring quality uniformity during manufacture.

The study approached these and other problem areas through the following group of tasks:

1. Reference flight and environmental conditions and loads were defined, representative of lift body vehicles.

2. Thermal stress analyses were performed for candidate ceramic materials, using high speed computer techniques, to establish analytical performance references for these materials and to define the desired pore geometry to satisfy thermal and structural needs.

3. Thermal shock tests were conducted to compare with the analytical results.

4. Heat shield design concepts were developed for the lift body surfaces.

5. Brittle material design studies were made to determine approaches for defining material variability and design strength allowables.

6. Manufacturing process and inspection techniques were reviewed to determine potential for achieving and assuring adequate material uniformity.

This summary report is complimented by Reference 1, which was prepared under the same study program and provides a more detailed presentation of the technical data.

II. REFERENCE DESIGN DATA

A lifting body reentry vehicle configuration, shown in Figure 1, was selected to establish a design environment for the ceramic heat shield. This configuration was selected as representative of vehicles offering maneuverable reentry flights. The extended time period of reentry required by such configurations increases the need for radiation rejection of aerodynamic heat and thereby provides conditions appropriate for potential use of ceramic heat shields.

The vehicle surfaces were classified into two categories, according to the severity of local pressures and temperatures. This was done to facilitate definition of environmental conditions and loads, and to aid in establishing appropriate designs for the heat shield sections. Accordingly, as illustrated in Figure 1, the entire vehicle undersurface between the horizontal centerlines as well as surfaces forward of station 48 inches (1.22 m) were considered high pressure and high heating zones, while the remaining lift body surfaces were considered relatively low pressure heating zones The base section and the control surface were not included in this study

A. Reentry Trajectories

Three reentry trajectories were selected to define the range of time, temperature, and pressure conditions required to establish environmental design criteria. The reentry flight regimes studied were L/D_{min}, L/D_{max}, and an abort reentry.

The three reentry flights are described in Figures 2, 3, and 4, which present altitude, velocity, dynamic pressure, and stagnation point heating rate data, based on a nose diameter of one foot (0.304 m) Figures 5, 6, and 7, show the radiation equilibrium temperatures at various locations along the lower vehicle centerline under the same flight conditions. Reference 2 describes the methods used in determining heating rates and pressures.

A review of Figures 2 through 7 offers the following comparison of environmental conditions of the three trajectories. All of the trajectories attain about equal maximum radiation equilibrium temperatures, but the abort trajectory results in the highest temperature rise rate, 55°F/second (30.5°K/second), as seen in Figure 7. The L/D_{max} trajectory provides the longest period of reentry (over one hour), while the L/D_{min} reentry develops the highest free stream dynamic pressures.

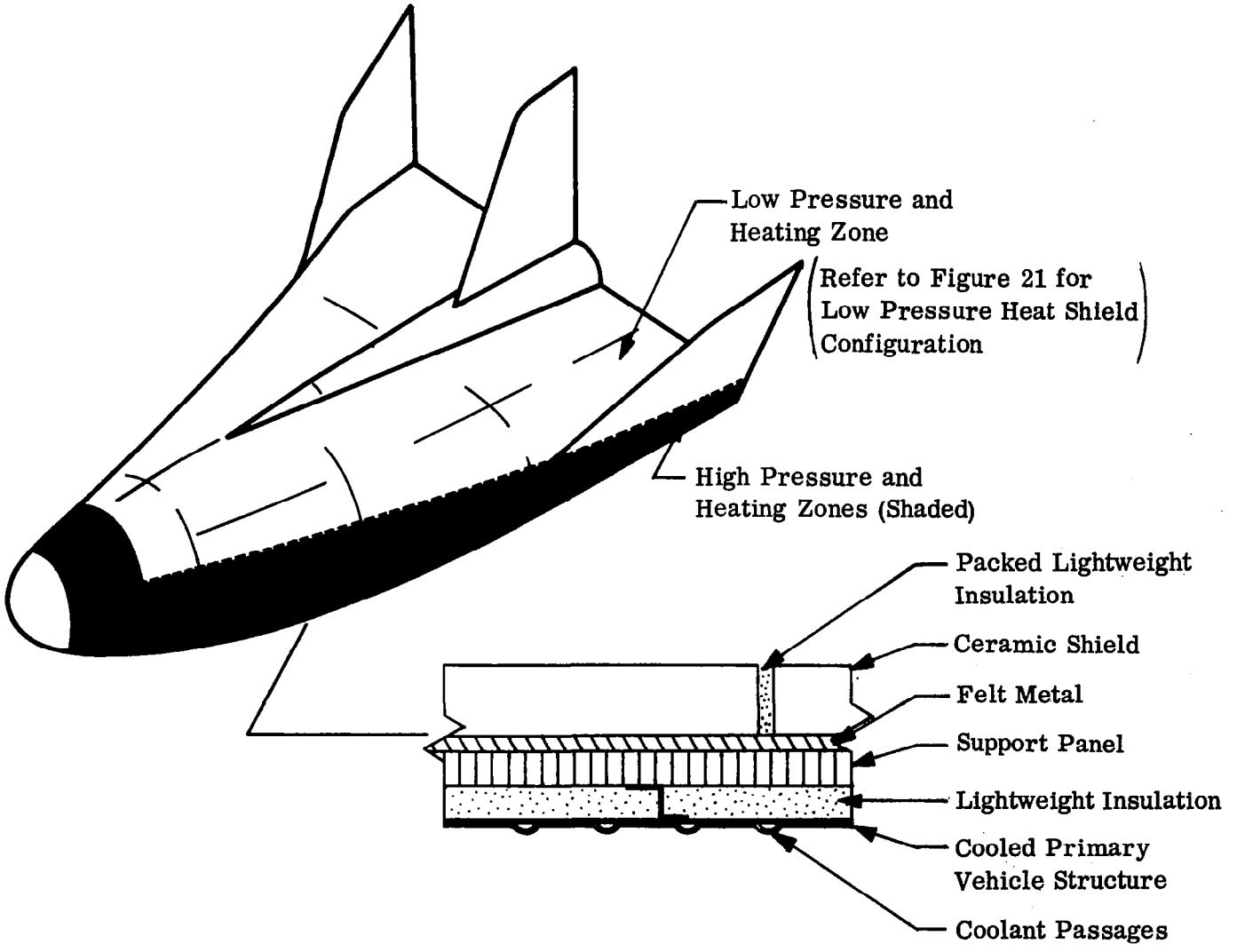

Figure 1. Representative Lifting Body Configuration

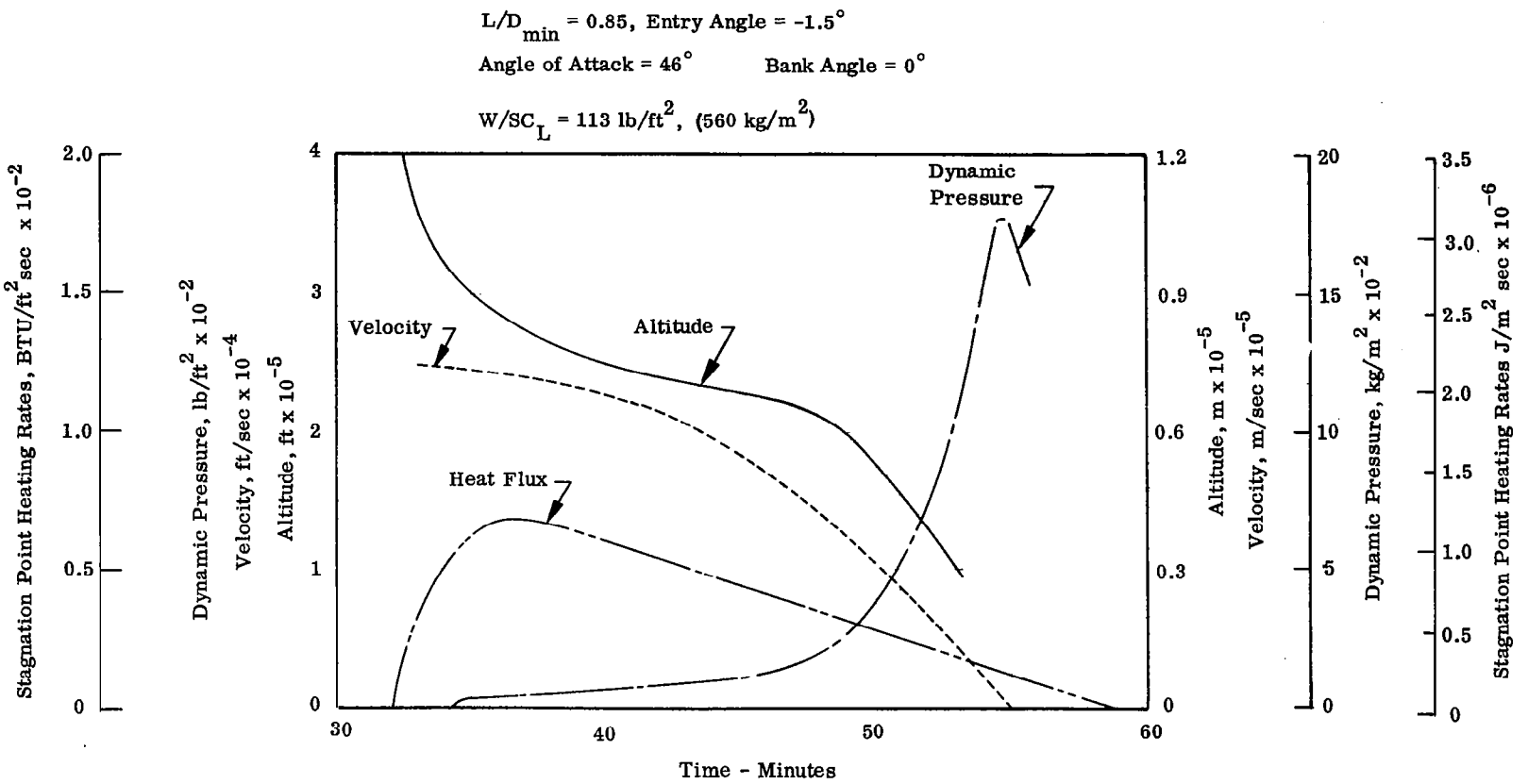

Figure 2. Reentry Trajectory For Lifting Body at L/D_{min}

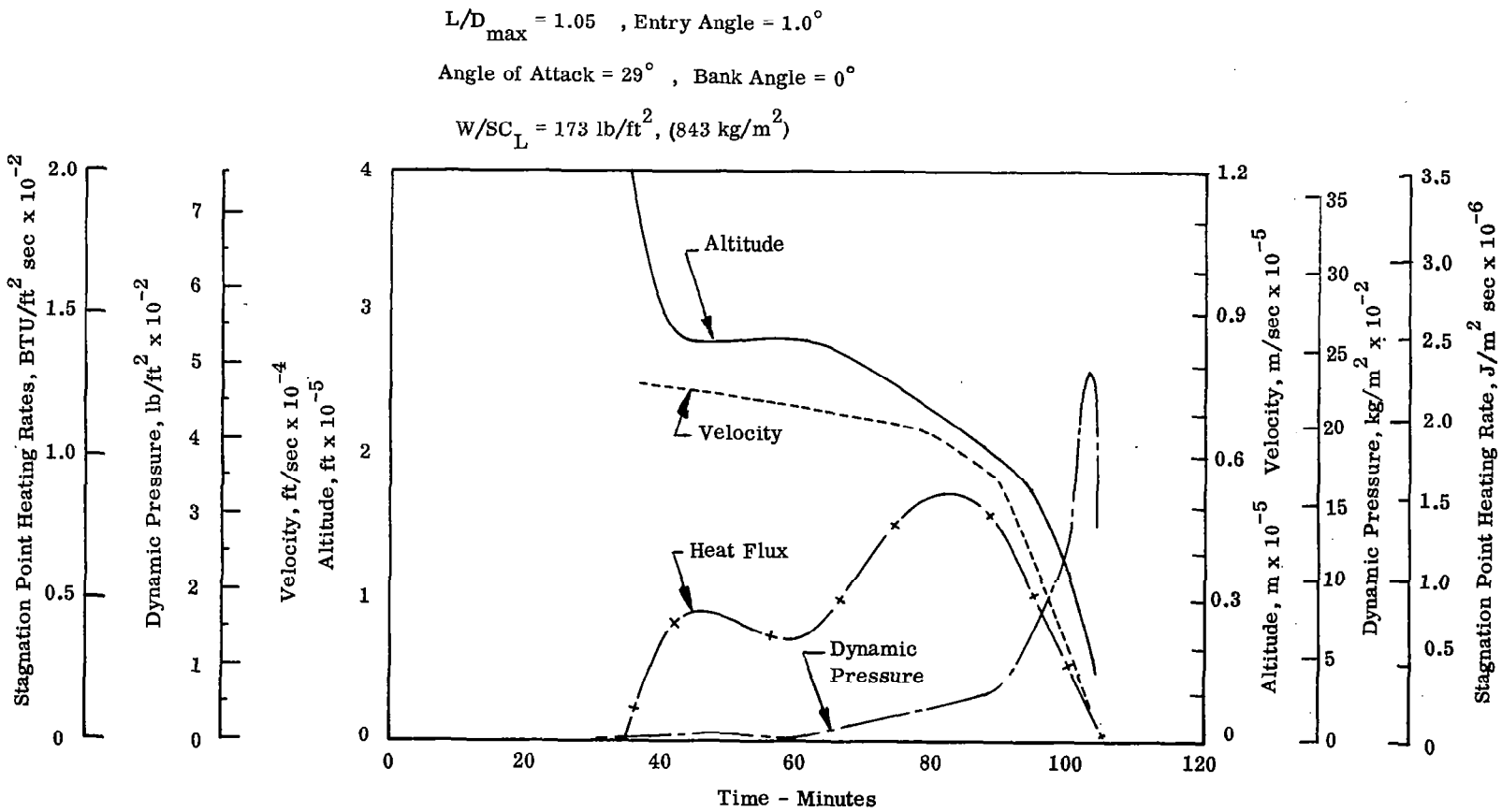

Figure 3. Reentry Trajectory For Lifting Body at L/D_{max}

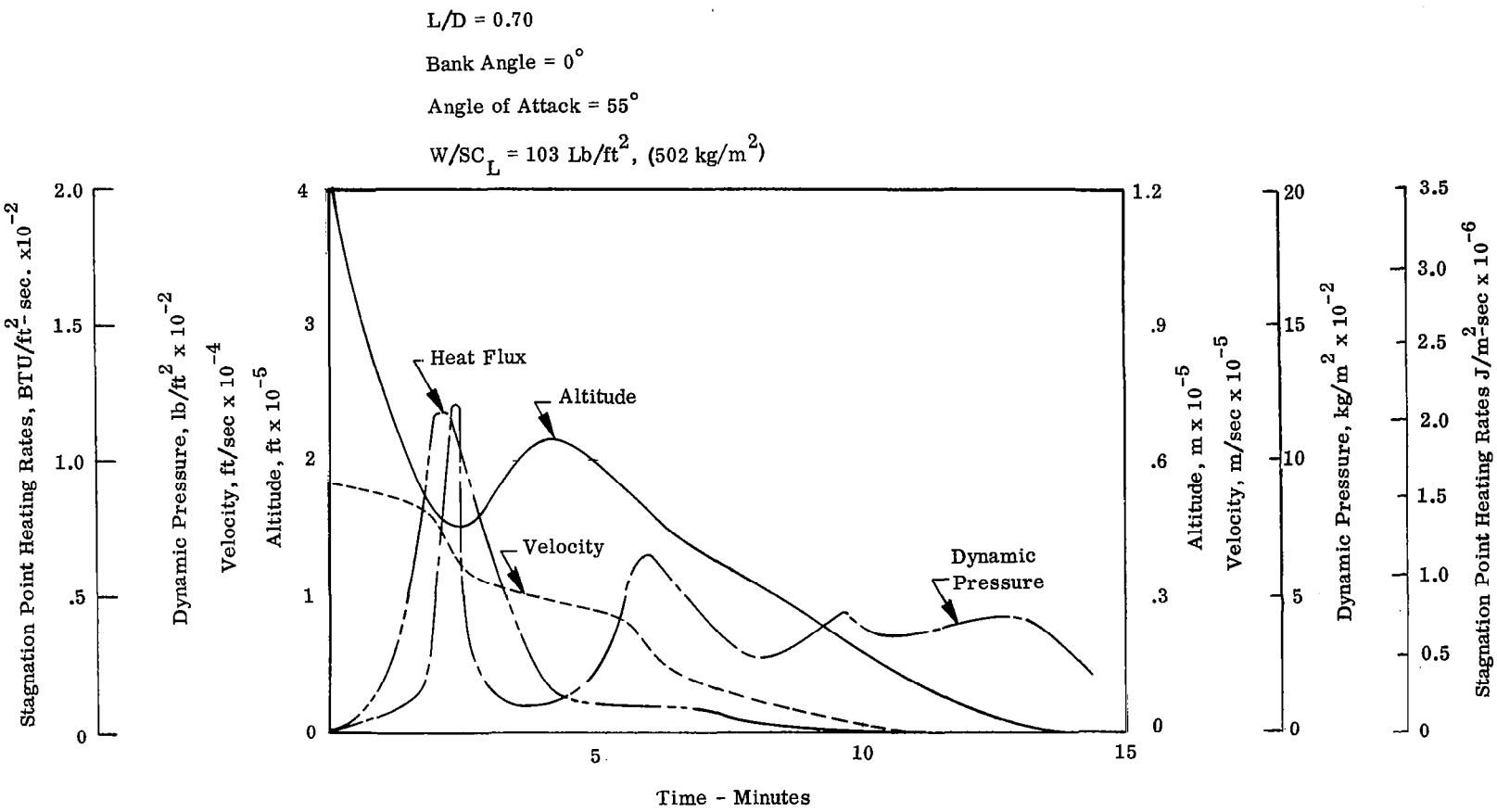

Figure 4. Trajectory For Abort Reentry

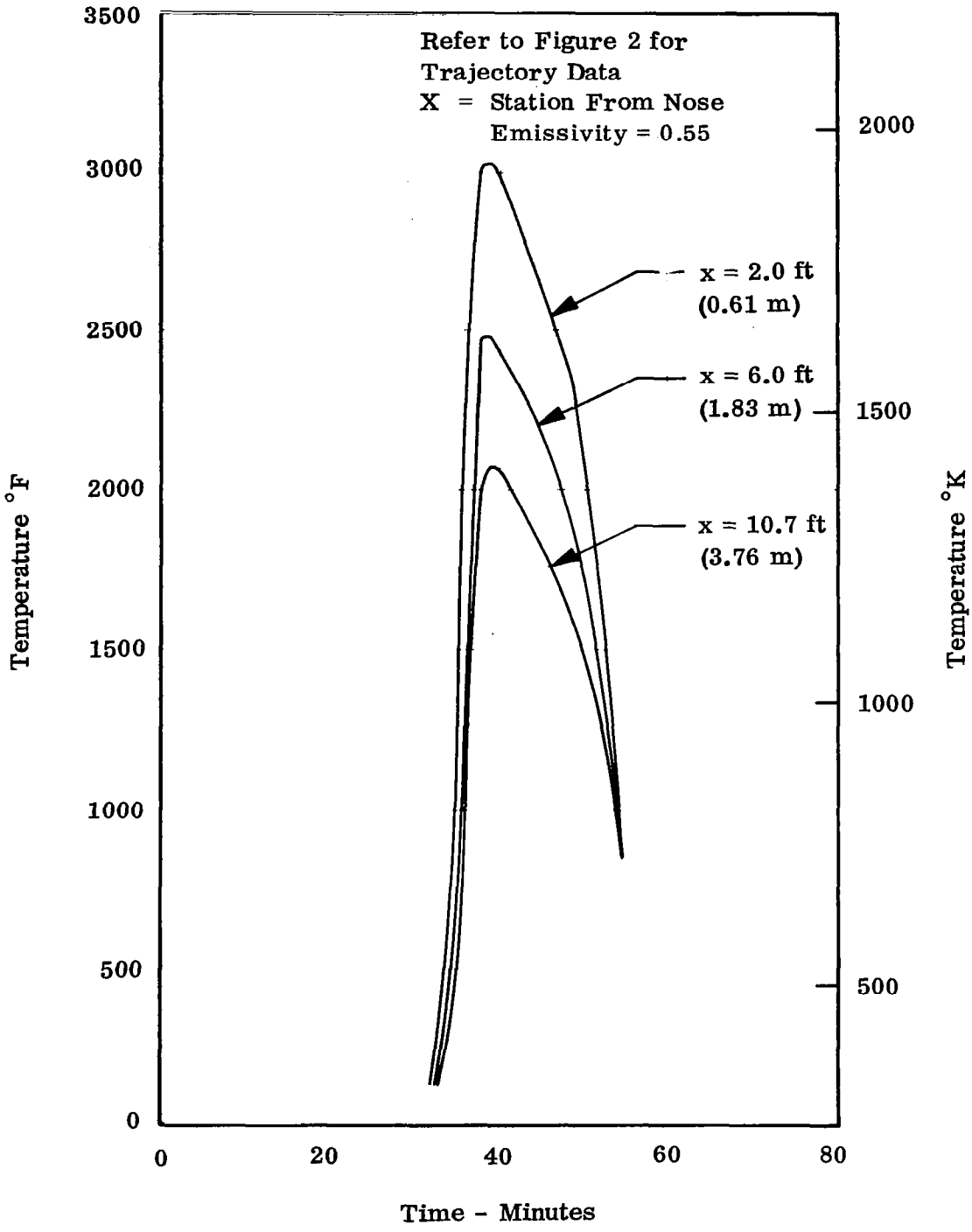

Figure 5. L/D_{min} Reentry Radiation Equilibrium Temperatures

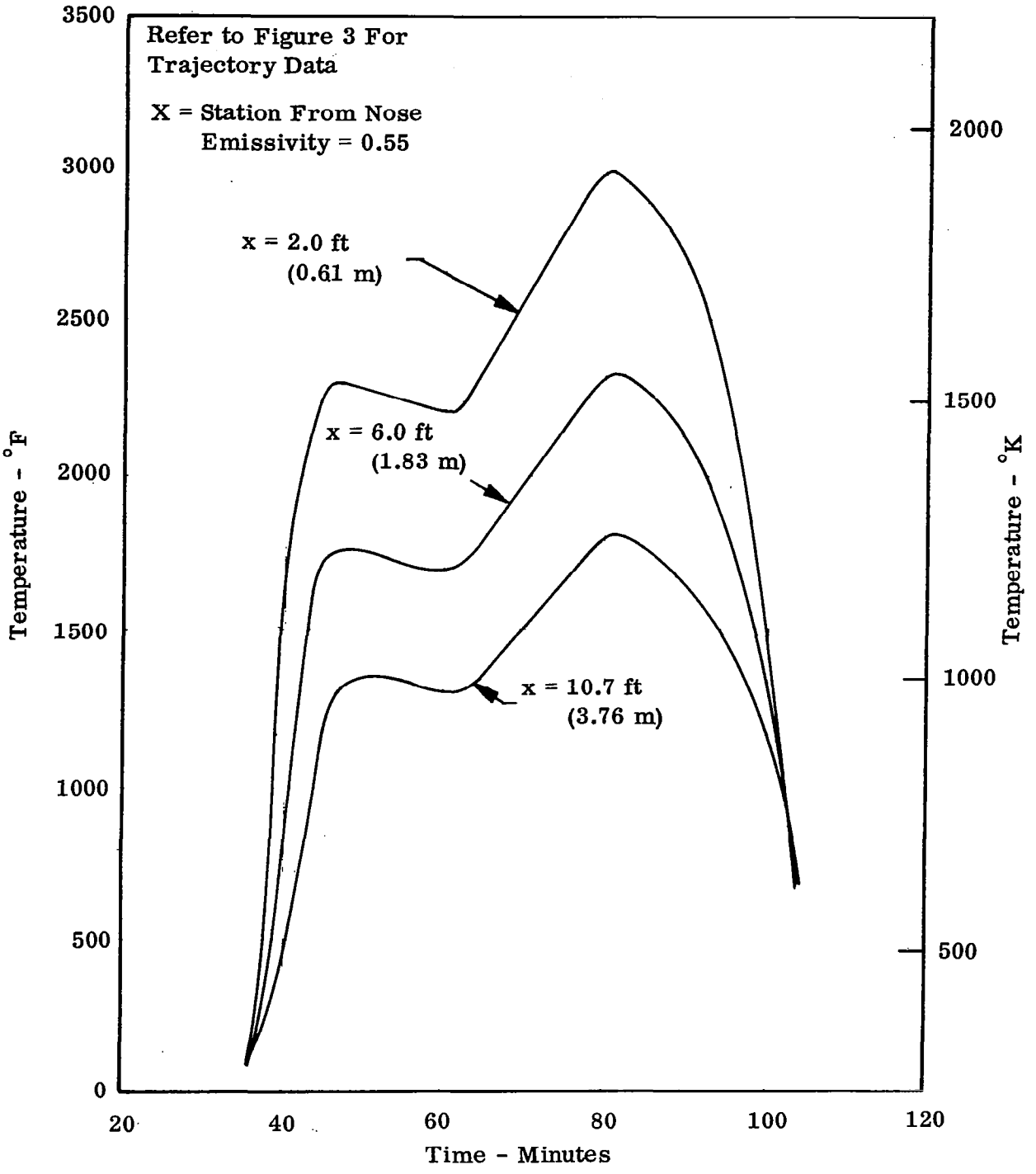

Figure 6. L/D_{max} Reentry Radiation Equilibrium Temperatures

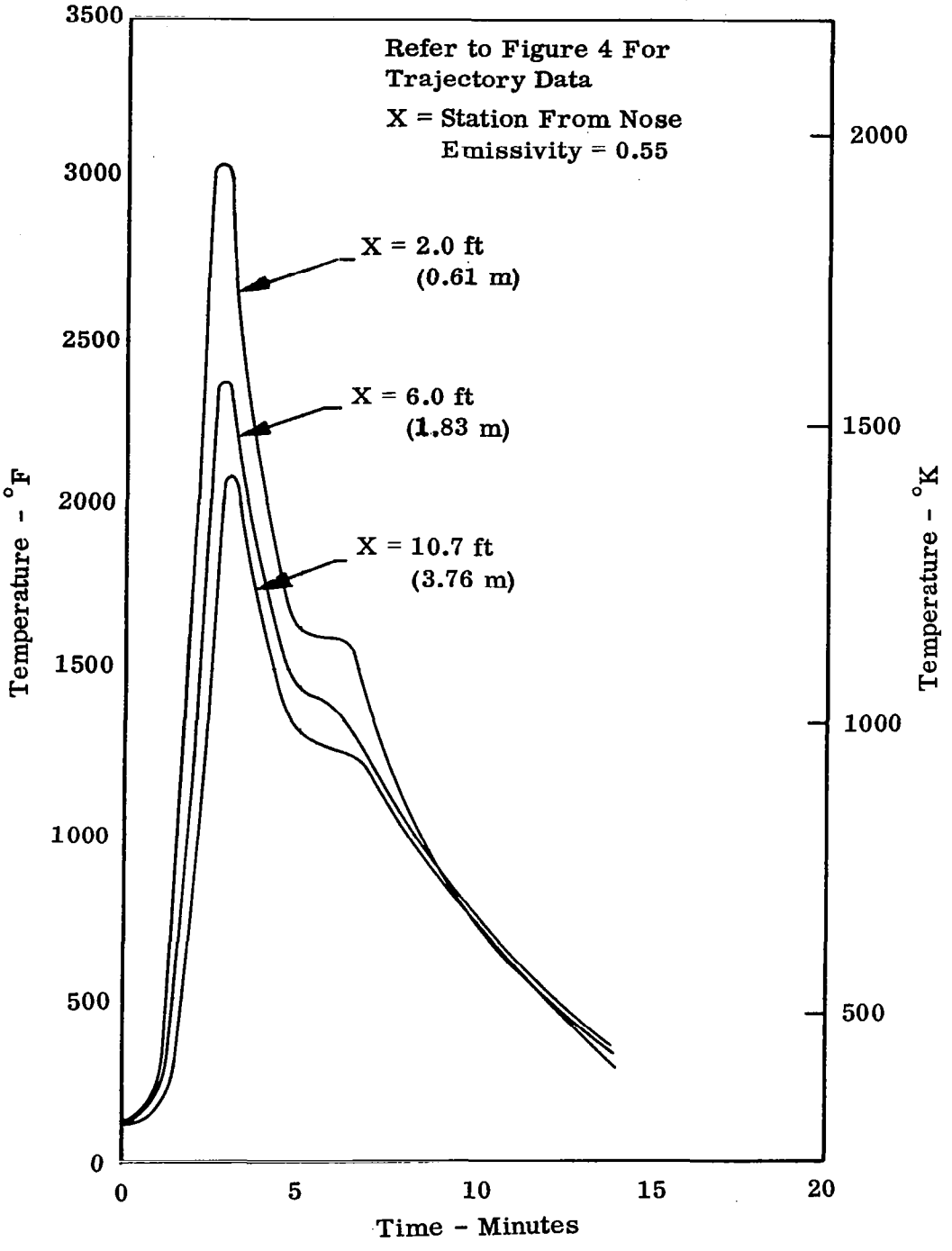

Figure 7. Abort Reentry Radiation Equilibrium Temperatures

B. Design Load Conditions

Table I summarizes the design loads selected for the high and low pressure sections of the vehicle. The assumptions used in the development of the design loads are described below:

1. Reentry pressure-temperature loads for the high pressure section.

Using the X = 2 feet (0.61 m) station along the bottom centerline as representative of the high pressure section of the vehicle, the abort trajectory provided the most severe combination of high temperature and pressure loading, equal to 3050°F (1950°K) and 390 lb/ft^2 (1900 kg/m^2) normal pressure. At the same location, the L/D_{min} reentry provided the highest normal surface pressure, 533 lb/ft^2 (2595 kg/m^2).

2. Reentry pressure-temperature loads for the low pressure section.

The X = 4-16 feet (1.22 - 4.9 m) locations above the horizontal centerlines were calculated to experience maximum surface pressure of 93 lb/ft^2 (454 kg/m^2) during the abort reentry. As a conservative assumption, the maximum temperature of the X = 6 feet (1.83 m) location at the bottom centerline, approximately 2400°F (1585°K) from Figure 7, was combined with the above pressure determination to establish the most severe pressure - temperature design conditions for the low pressure vehicle section.

Maximum reentry normal pressure was found to occur during L/D_{min} reentry and equaled 106 lb/ft^2 (516 kg/m^2).

3. Reentry inertial loads.

The maximum axial inertial load factor during reentry is 4.4g, occurring during abort reentry, as shown in Figure 8. Lateral accelerations were not considered.

4. Boost loads.

While a variety of boost flight paths are available, the conditions of Table I were based on an 8 g load factor which would be appropriate for a boost system such as the Atlas-Centaur or Titan III - Centaur.

5. Vibration and acoustical environments.

Typical booster engine vibration inputs and boundary layer acoustical inputs to the reentry vehicle were selected (Reference 3), as shown in Figure 9.

TABLE I SUMMARY OF ENVIRONMENTAL DESIGN LOADS

	Normal Pressure lb/ft^2	(kg/m^2)	Outer Surface Temperature °F	(°K)	Inertial Axial Load Factor	Acoustical Input	Vibration Input
A. Reentry Loads, High Pressure-Temperature Vehicle Surfaces							
Most Severe Combined Pressure-Temperature Conditions	390	1900	3050	1950	4.4g	138db	
Maximum Normal Pressure	533	2595					
B. Reentry Loads, Low Pressure-Temperature Vehicle Surfaces							
Most Severe Combined Pressure-Temperature Conditions	93	454	2400	2859	4.4g		
Maximum Normal Pressure	106	516					
C. Boost Load Conditions							
Maximum Acceleration	64	312	500	533	8g		135db
Maximum Normal	252	1225	Low		1.5g		

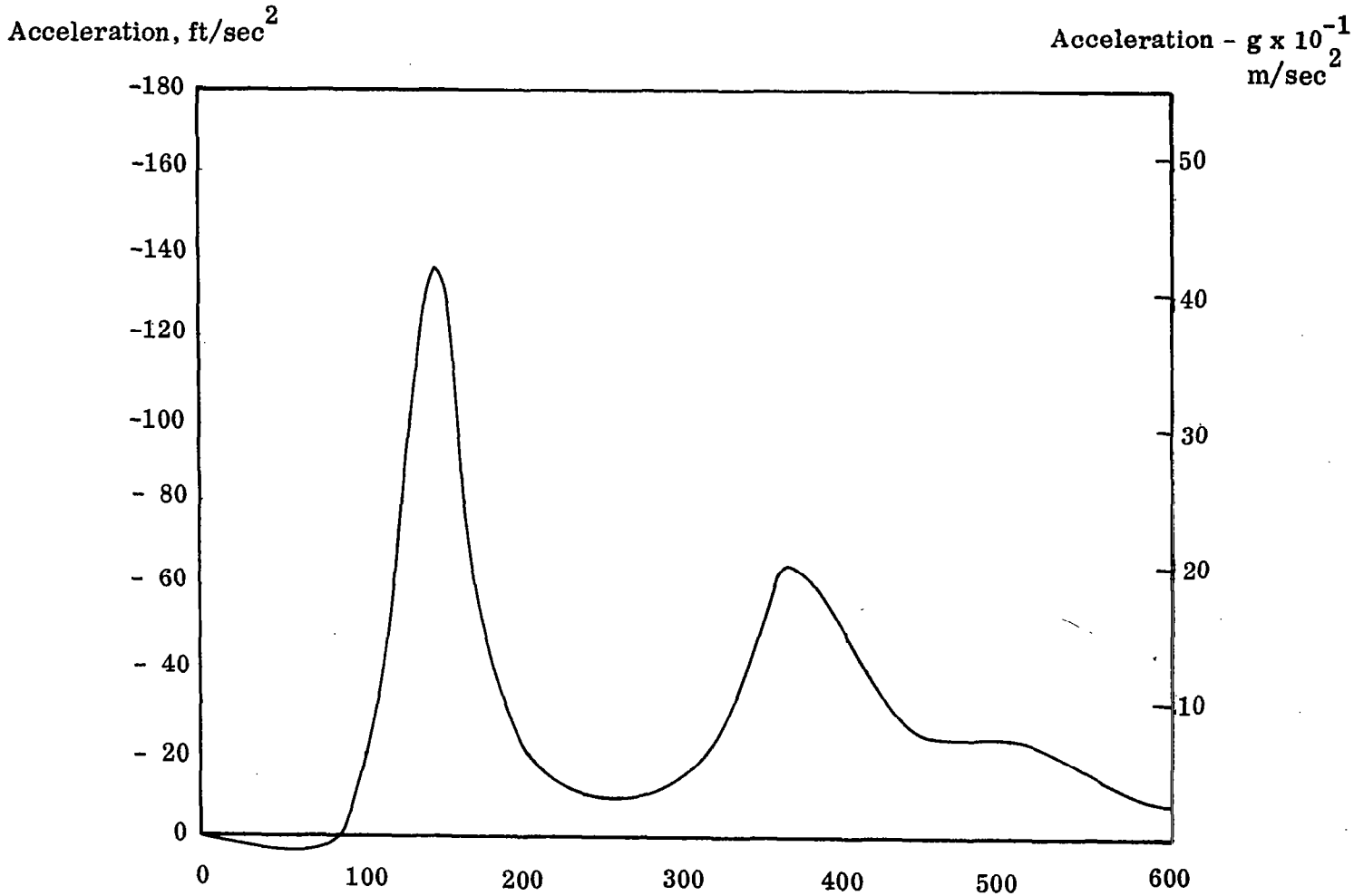

Figure 8. Abort Reentry Trajectory Acceleration

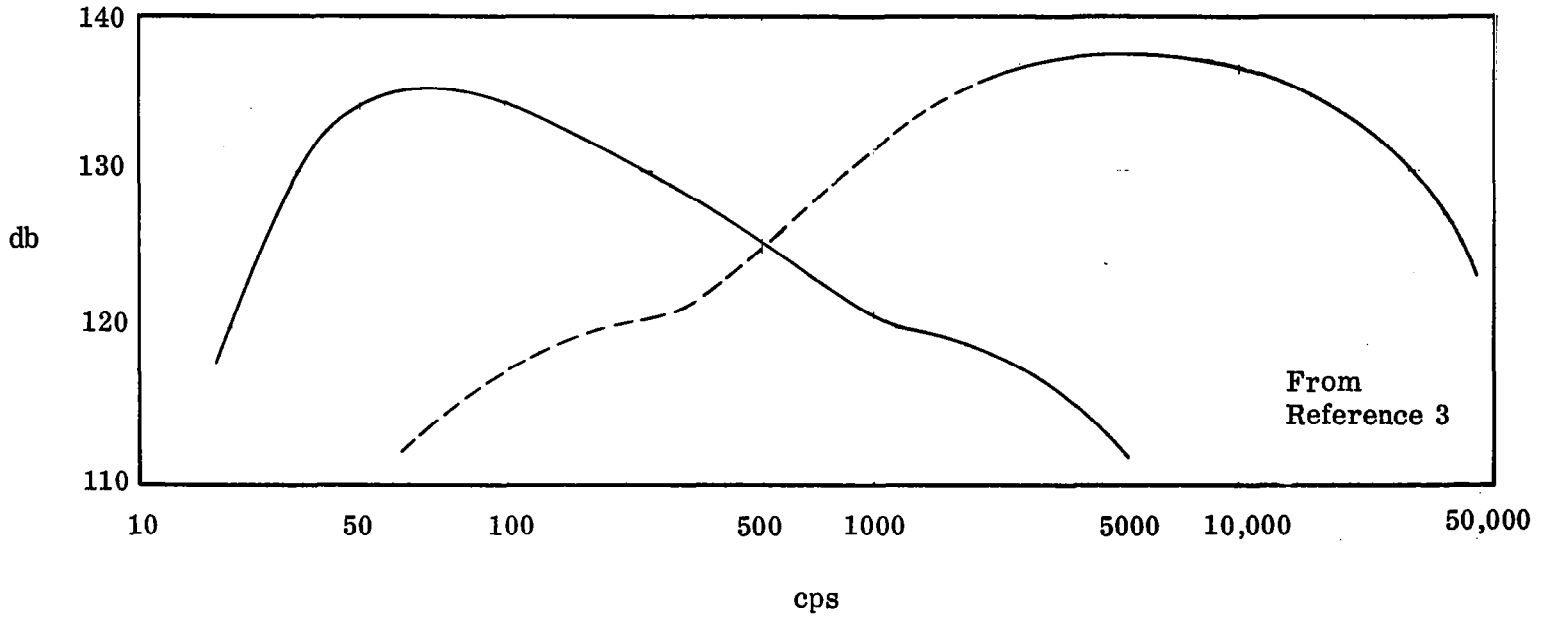

Boundary Layer Noise: SPL = 142 db (Overall)

Dashed Line = Values From Measurements During Flight (WADC)

Solid Line = Values From Wind Tunnel Results (NACA)

SPL in db Referenced to 0.0002 Microbar

Booster Engine Noise at 100 feet (30.5 m) SPL = 140db (Overall)

Figure 9. Spectra of Booster Engine and Boundary Layer Noise

III. MATERIAL CANDIDATES AND SELECTION

Analytical and experimental methods were used to evaluate and select the heat shield materials. Thermal and structural analyses were performed to define a performance expectation or reference for each material. Thermal shock tests were then performed to provide a direct evaluation of the materials under repeated simulated reentry heating, and also to examine the accuracy of the analytical methods in predicting the performance of the porous structures.

A. Selection of Material Candidates

The selection of material candidates was based on overall application considerations including: favorable properties for resistance to thermal environments, existence of a reasonable amount of processing experience with potential ability to control microstructure, and reasonable cost.

In general, only oxide materials were considered because of their high degree of chemical stability in the maximum operating temperatures, 2400 to 3050°F (1585 to 1949°K). Table II lists the materials selected for application study, together with the reasons for their consideration.

B. Analytical Procedures

Literature data were utilized in establishing thermal and mechanical properties of the materials as functions of temperature and porosity. Since test information is comparatively scarce for high porosity ceramics, it was found necessary to interpolate between test points, or apply empirical or analytical relationships to approximate properties at porosities and temperatures of interest. Representative expressions for relating porosity and temperatures to strength and modulus of elasticity are presented in Appendix A.

One-dimensional transient temperature and thermal stress solutions were developed for each of the candidate materials, using the first four minutes of the abort trajectory as the environmental heating condition. The geometry analyzed consisted of a plate of selected thickness, and infinite in size in the plane of the plate so that full thermal stresses could be determined. The thermal and mechanical properties used in the study considered the effects of porosity and temperature. The computer methods for thermal and thermal-stress analyses and the boundary conditions are described in Appendix B.

TABLE II

CRITERIA FOR SELECTING MATERIAL CANDIDATES

Materials	Selection Considerations
A. Service to 3050°F (1949°K)	
1. Alumina Al_2O_3	Extensive process and test data. Stable at operating temperatures. Porous forms available over wide density range. 25-85 lb/ft^3 (399-1355 kg/m^3).
2. Aluminum Silicate $3Al_2O_3.2SiO_2$ (and with excess Al_2O_3)	Lower elastic modulus and thermal expansion coefficient than alumina; commonly available at low cost in density ranges of 40-70 lb/ft^3 (640-1116 kg/m^3). Properties entering into analysis are also representative of many other silicates.
3. Zirconia ZrO_2 (Stabilized)	Extensive process and test information; high melting point. Low modulus of elasticity. Available at moderate cost.
4. Fused Silica SiO_2	Very low thermal expansion coefficients. Low weight of material permits use at lower porosity fractions with less degradation in strength. Demonstrated good thermal and mechanical properties in nose cone tests. Thermal stresses expected to be low in comparison with material strength, thus enabling a margin of safety design. Low cost material. Cristobolite formation believed to be slow under reentry conditions.
5. Zircon $ZrO_2 \cdot SiO_2$	Low thermal expansion coefficients, approximately 1/3 of those for zirconia. Low modulus of elasticity. Good chemical stability.
6. Spinel $MgO \cdot Al_2O_3$	Lower elastic modulus than alumina.
B. Service to 2400°F (1585°K)	
1. Alumina 2. Aluminum Silicate 3. Fused Silica	Refer to Part A
4. Lithia-Alumina-Silicate Li_2O-Al_2O_3-SiO_2	Very low thermal expansion coefficients. Low cost, available in forms such as Pyrocerams, etc. Excellent thermal shock resistance.
5. Cordierite $2MgO \cdot 2Al_2O_3 \cdot 5SiO_2$	Low thermal expansion coefficients, low elastic modulus.

Weight and thermal determinations were developed to define module thickness and porosity ranges of interest for the candidate materials before conducting detailed thermal stress analyses to check structural adequacy. A plate thickness of 1/2 inch (.0127 m) together with a pore diameter of 0.015 inch (3.81 mm) were found to offer a good preliminary balance of weight and insulation properties for materials in the 25-85 lb/ft^3 (399 - 1355 kg/m^3) density range. Larger pore dimensions were found to be particularly detrimental to insulation properties, because of thermal radiation across the pores.

C. Analysis Results

Typical thermal and thermal stress analysis of the candidate materials are included in Appendix C. Reference 1 contains the detailed results of all the analyses performed.

Table III summarizes the results of the analytical evaluations of the candidate meterials. Table III shows that for the density ranges considered, the thermal stress parameter σ/σ_A is excessively high for most of the materials, thus predicting failure due to thermal shock conditions existing at vehicle station X = 2 feet (0.609 m).

Because of its low thermal expansion characteristics, fused silica of 50% density, however, shows maximum calculated stress to be considerably below the material strength. It appears, therefore, that lower densities can be considered for fused silica.

It is also to be noted from the results of Table III, that variable density designs incorporating dense surfaces at either the front face or front and back faces of the ceramic plate provided negligible improvements in thermal stress resistance as compared to uniform density plates. On the other hand, surface cuts arranged in a square grid pattern, significantly reduced the stress level in the plate. The thermal stress parameter for alumina was reduced by a factor greater than 6 by this change in geometry.

Although not calculated, it would appear from a comparison of values of the thermal stress parameter in Table III, that surface cutting would likely provide a satisfactory analytical outlook for several materials at a density of about 50 lb/ft^3 (799 kg/m^3), including aluminum silicate and zircon.

TABLE III CALCULATED THERMAL STRESSES OF CANDIDATE MATERIALS DURING ABORT REENTRY AT THE X = 2 feet (0.609 m) UNDERSURFACE CENTERLINE

MATERIAL(1)	LOCATION DENSITY DISTRIBUTION	DENSITY lb/ft^3,	DENSITY kg/m^3	MAXIMUM VALUE OF THERMAL-STRESS PARAMETER σ/σ_A (2)
1. Alumina	Uniform	85	1355	-9.45
2. Alumina	Uniform	50	799	-16.685
3. Alumina	(a) Densified Outer Surface, 0.05 inch (1.2 mm) thick	150	2397	-13.570
	(b) Module Core, 0.40 inch (10 mm) thick	50	799	
	(c) Densified Back Surface 0.05 inch (1.2 mm) thick	150	2397	
4. Alumina	(a) Densified outer Surface 0.05 inch (1.2 mm) thick	150	2397	-11.992
	(b) Remainder of Module 0.45 inch (11.5 mm) thick	50	799	
5. Alumina	Uniform Density Outer Surface Cut to a Depth of 0.100 inch (2.5 mm) in a square grid pattern with 0.50 inch (12 mm) spacing of grid cuts	50	799	-2.625
6. Aluminum Silicate	Uniform	50	799	-6.167
7. Fused Silica	Uniform	68.5	1094	0.059
8. Spinel	Uniform	50	799	10.365
9. Zircon	Uniform	70	1116	-1.889

(1) Pore Diameter in all cases is 0.015 inch (0.38 mm)

(2) σ/σ_A is the ratio of stress to allowable stress

Negative numbers denote compression stress

Positive numbers denote tensile stress

Table IV presents the analytical evaluation of materials for the low pressure-temperature vehicle zones which would attain temperatures to 2400°F (1585°K). The low thermal expansion materials, cordierite and spodumene, appear satisfactory and from an analytical standpoint even lower densities may be considered other than those used. Fused silica, which was calculated to be adequate for the high temperature vehicle zones, would also be a likely candidate for the lower temperature zones.

D. Experimental Evaluation of Materials

Thermal shock testing was the primary means of experimentally evaluating the candidate materials. This testing method is appropriate to the heat shield design approach utilized (refer to Section IV which requires that the ceramic modules be supported in such a manner that mechanically induced stresses are eliminated or greatly reduced). A very limited number of bend tests were performed and these were intended to offer a comparison with tne theoretical material properties used in the thermal stress analyses.

1. Description of Test Materials.

Table V describes the materials obtained for testing. Materials A, B, C, and D are highly porous with a structure resembling a lacy network; this construction is illustrated in Figure 10.

Material E (see Figure 11) shows an experimental specimen with the same type of microstructure, but constructed to determine whether smaller pore diameters could be achieved. The average diameter was reduced to less than half of specimens A through E, demonstrating that there is wide potential versatility in pore geometry for the lacy constructions. Material E was not tested, however, since the process was not set up for the purpose of constructing reproducible test specimens.

The aluminum silicate specimens, Material F, consisted of sintered hollow spherical particles as shown in Figure 12. This was an intermediate structure containing some open pores (between the particles) and some closed pores (within the particles).

Figure 13 presents a photograph of slip cast fused silica. This construction showed a considerable proportion of the closed pores.

TABLE IV CALCULATED THERMAL STRESSES OF CANDIDATE MATERIALS DURING ABORT REENTRY AT THE X = 6 feet (2.03m) UNDERSURFACE CENTERLINE LOCATION

MATERIAL (1)	DENSITY DISTRIBUTION	DENSITY lb/ft^3	DENSITY kg/m^3	MAXIMUM VALUE OF THERMAL STRESS PARAMETER σ/σ_A (2)
1. Cordierite	Uniform	40	639	0.204
2. Spodumene	Uniform	40	639	0.132
3. Spodumene	Uniform	40	639	0.132
4. Alumina	Uniform	50	799	-5.648
5. Alumina	Uniform. Density Outer Surface Cut to a Depth of 0.10 inch (2.54mm) in a square grid pattern with 1/2 inch (0.012m) spacing of grid cuts	50	799	-1.314

(1) Pore Diameter in all cases is 0.015 inch (0.38 mm)

(2) σ/σ_A is the ratio of stress to allowable stress

Negative numbers denote compression stress

Positive numbers denote tensile stress

TABLE V IDENTIFICATION OF TEST MATERIALS

CODE		DENSITY		CONSTRUCTION	AVERAGE PORE DIAMETER		MANUFACTURER
IDENTIFICATION	DESCRIPTION	lb/ft^3	kg/m^3		inch	mm	
A	96% Alumina	48	766	Open pore, lacy, see Figure 10	0.018	0.457	American Lava Corp.
B	99% Alumina	50	799	Same	0.018	0.457	American Lava Corp.
C	Zirconia Stabilized	35	559	Same	0.018	0.457	American Lava Corp.
D	Zircon	50 & 24	799 & 383	Same	0.010	0.254	American Lava Corp.
E	Alumina	40	639	Open Pore, lacy see Figure 11	0.004-0.010	0.102-0.254	Bell Aerosystems
F	Aluminum Silicate 63.5% Al_2O_3-32.7% Silica	50	799	Sintered Spherical particles, 0.050 inch (1.2mm) diameter See Figure 12	Irregular pores		A. P. Green Co.
G	Fused Silica	50 & 25	799 & 399	Partially closed pore Construction. See Figure 13	0.006-0.007 0.020	0.152-0.178 0.508	Glassrock Products

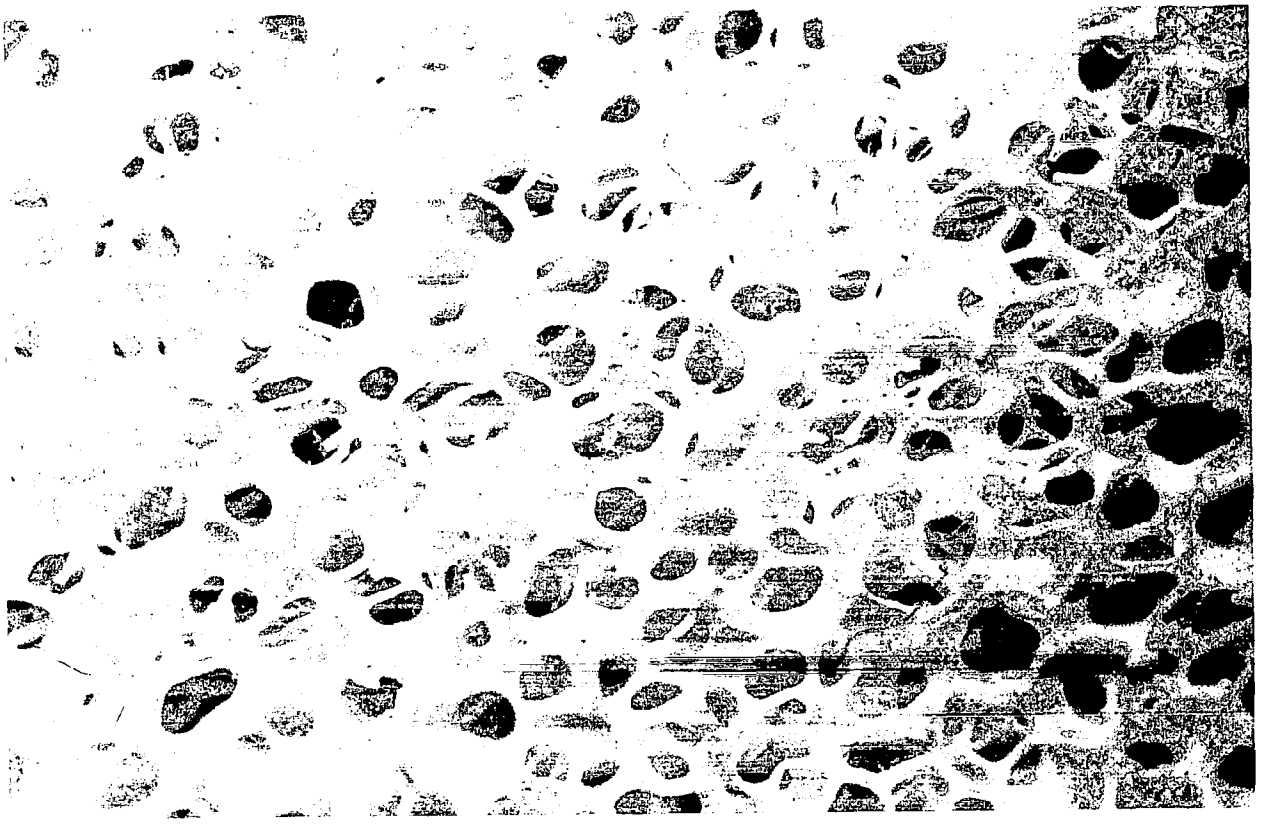

Magnification 20X

Figure 10. Structure of Material C, Zirconia

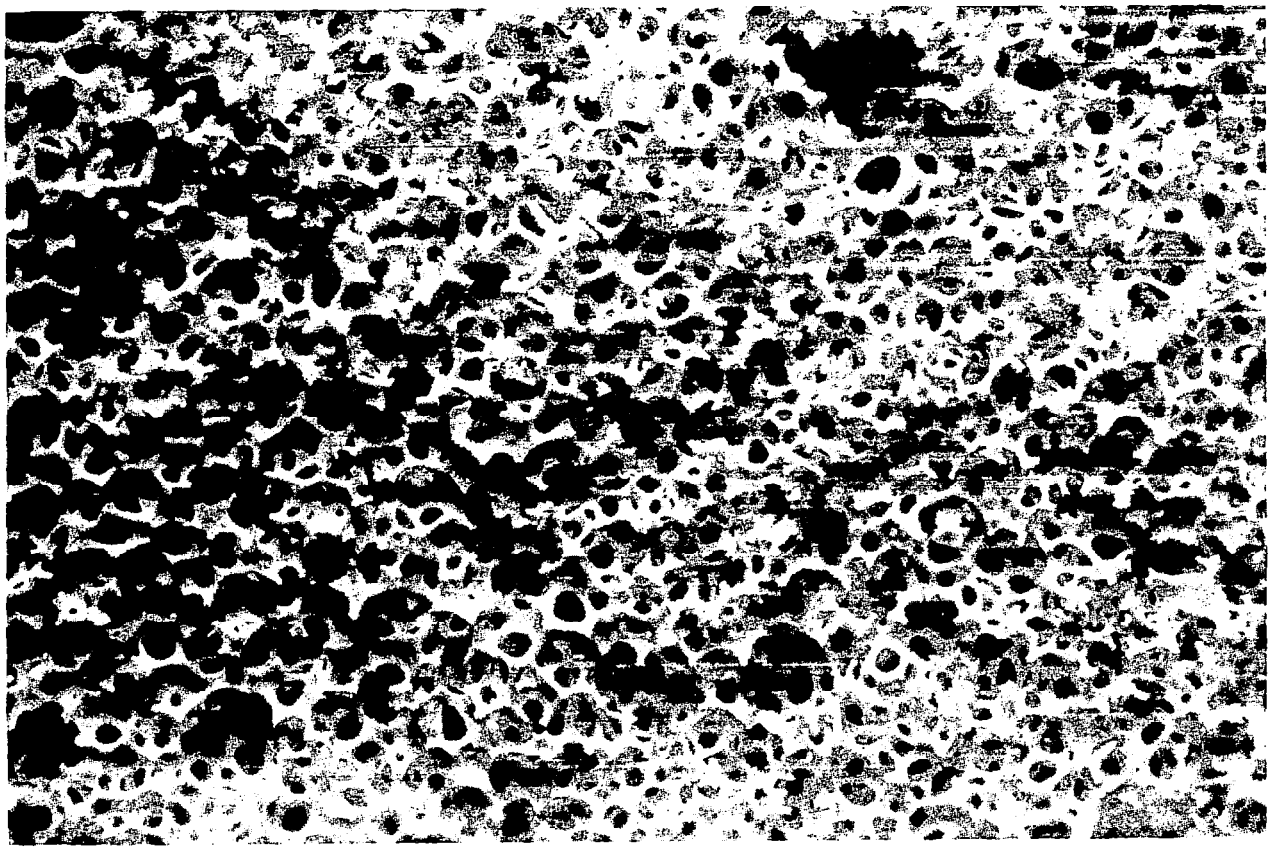

Magnification 20X

Figure 11. Structure of Material E, Alumina

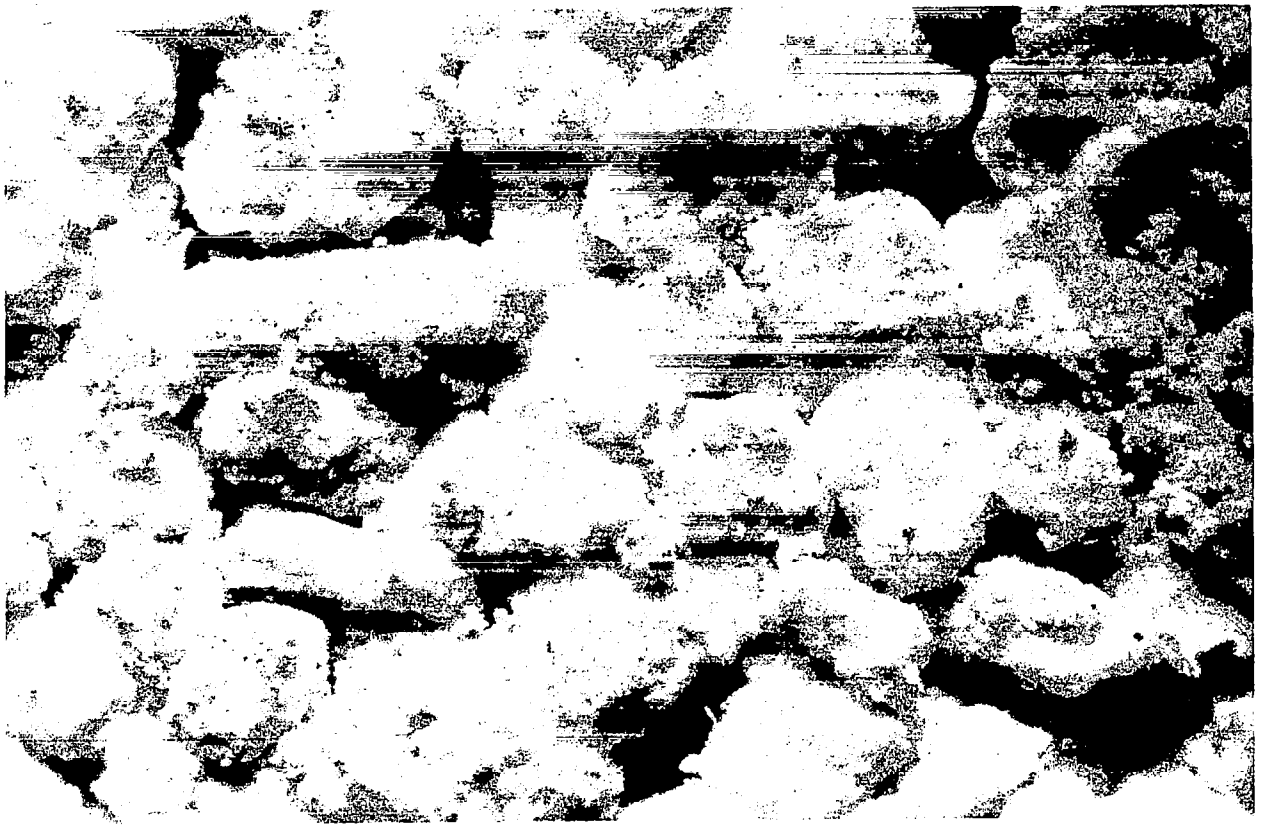

Magnification 20X

Figure 12. Structure of Material F, 63.5% Alumina - 32.7% Silica

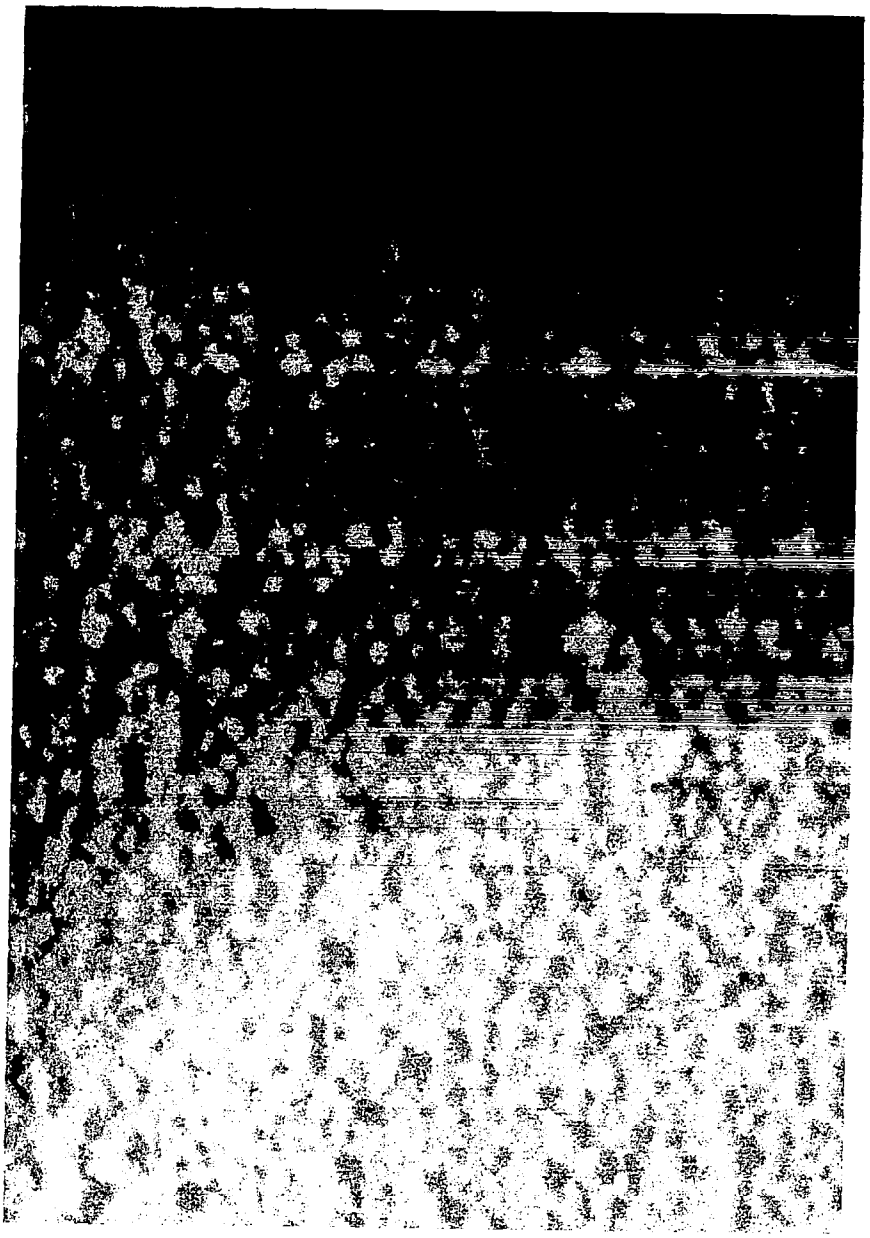

Magnification 25X

Figure 13. Micrograph of Fused Silica, Material G Density 50 lb/ft^3 (799 kg/m^3)

2. Thermal Shock Test Method.

Thermal shock testing was conducted to simulate the most severe vehicle heating environment which occurs during abort reentry. A temperature rise rate of 55 °F/sec (30.5 °K/sec), applied for one minute, approximates the abort reentry and this heating schedule was adopted as the nominal test environment.

The specimens, 4 x 4 inches wide (0.102 x 102 m) and 1/2 to 3/4 inch thick (0.012 to 0.019 m), were held at the edges by means of flexible insulation material so that essentially no mechanical restraint was provided with respect to the thermal expansions of the specimens. This conforms to the design concepts of Section IV which eliminate restraint of the ceramic modules at the attachments of the structure.

The heating facility consisted of an oxyacetylene burner mounted on a lathe. The lathe mechanisms enabled movement of specimens with respect to the burner to control heating intensity. The burner nozzle was capable of quick rotation upward or downward so that the flame could be suddenly applied to the specimens, or quickly removed if desired at the end of the test run.

Oxygen and acetylene supply rates were measured and kept constant during all runs. Specimen front face and back face temperatures were measured and continuously recorded. Thermocouples were attached at about the center of the specimen faces, with the front face thermocouple wires placed through a small diameter hole in the specimen. The thermocouple was in the plane of the surface and exposed to the flames.

Figure 14 illustrates the heating method. The flame produced radial temperature gradients on the specimen surfaces, a situation which is more severe than the expected flight condition. Maximum temperatures occurred in the center of the specimens over a 2-inch (0.051 m) diameter, while temperatures near the edges were lower by 500 to 1000°F (278-556 °K). A second factor which increased the test severity was that the initial temperature rise considerably exceeded the desired rate of 55°F/second (30.5°K/second) although a test procedure was evolved which provided an average temperature rise at the desired rate over a 60-second period.

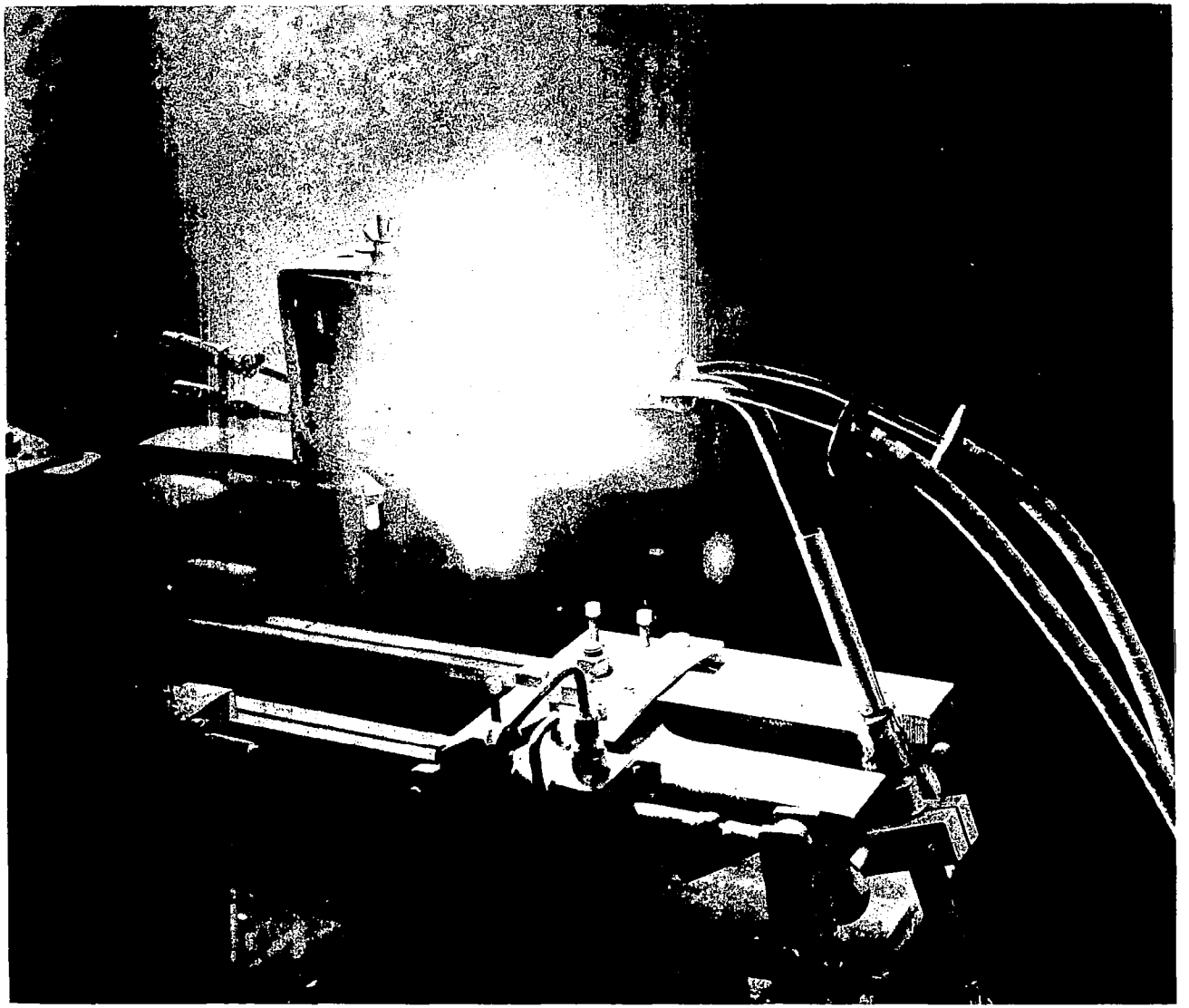

Figure 14. Oxyacetylene Thermal Shock Unit

3. Results of Thermal Shock Tests.

Table VI summarizes the results of the tests, and Figures 15 and 16 present the outer and back surface temperatures during thermal shock testing.

Three materials demonstrated excellent thermal shock resistance and survived 12 heating cycles with little or no damage. These were; 99% alumina, 50 lb/ft^3 (384 kg/m^3) density; zircon, 24 lb/ft^3 (384 kg/m^3) density; and fused silica, 25 and 50 lb/ft^3 (399 and 799 kg/m^3) density. The fused silica specimens before and after test are shown in Figure 17.

The aluminum silicate specimens survived 4 to 12 heating cycles, while zirconia failed on the first cycle.

While uniform geometry 96% alumina specimens survived 5 to 6 cycles, one specimen, in which surface cuts were made in the form of a square grid pattern to relieve outer surface stresses, survived 10 cycles. Cracks did not propagate from the base of the surface cuts.

X-ray diffraction studies were made to determine whether crystalline changes occurred in the specimens during the thermal tests. It was found that the crystobolite content increased at the surface of the fused silica specimen from about 10% to about 30%. No changes were detected in the zircon, zirconia, alumina, and aluminum silicate specimens.

4. Modulus of Rupture and Modulus of Elasticity Tests.

Bend tests were performed on specimens cut from the porous ceramic materials to determine the moduli of rupture and elasticity. The specimens were 3/8 x 3/8 x 4 inches (0.0095 x 0.0095 x 0.101m) and were tested by 4-point loading. Results are presented in Table VII together with a comparison of values determined from the literature and corrected for porosity. In general, the measured moduli of rupture were lower than the tensile test values obtained from the literature. The experimental elastic modulus for fused silica was higher, whereas the zirconia and aluminum silicate values were lower. The differences between measured and literature properties may arise from difference in test method, effects of different material processing conditions, and errors in determining the effects of porosity.

TABLE VI PERFORMANCE OF MATERIALS IN THERMAL SHOCK

Material	Composition	Density lb/ft^3	Density kg/m^3	Specimen Number	Thickness of 4 x 4 in. (0.702 x 0.102m) plates		Number of Test Cycles	Damage
					inches	mm		
A	96% Alumina	48	766	1	1/2	12	6	Failed after 6 cycles. Cell walls broke and edges showed some fusion.
				2	3/4	19	5	Broken accidentally after 5th cycle.
				3	3/4 [with 1/16 in. (1.6 mm) depth surface cuts in 1/2 in. (12mm) square pattern]	19	11	Cracks were noticed after the 10th cycle and a grid section spalled off during the 11th cycle. The specimen retained structural integrity.
B	99% Alumina	50	799	1	3/4	19	12	Survived 12 heating cycles, retaining structural integrity. Some surface spalling occurred after the 8th cycle.
				2	3/4	19	12	Survived 12 heating cycles. Slight surface spalling after the 8th cycle.
C	Zirconia	35	559	1	1/2	12	1	Failed on first heating cycle. Large transverse cracks.
				2	1/2	12	1	Failed on first cycle.
D(1)	Zircon	24	383	1	3/4	19	12	Survived 12 cycles with no crack damage.
				2	3/4	19	12	
(2)	Zircon	50	799	1	3/4	19	5	Progressive cracking, became severe after 3 cycles, and caused complete failure after 5 cycles.
				2	3/4	19	5	
F	Aluminum Silicate	50	799	1	1/2	12	12	Specimen survived 12 cycles. Progressive cracking noted along several lines. Large reduction of bend strength as a result of cracks.
				2	1/2	12	4	Specimen failed on fourth cycle. Large transverse cracks developed.
G (1)	Fused Silica	25	399	1	3/4	19	12	No crack damage. Surface fusion. Increase in cristobolite content at surface.
				2	3/4	19	12	
(2)		50	799	1	3/4	19	12	
				2	3/4	19	12	
A (2)	96% Alumina	48	766	1	3/4	19	4	Specimen subjected to only four heating cycles. No apparent thermal damage to specimen.

○ Aluminum Silicate, Material F
● 96% Aluminum Oxide, Material A, Specimen 1
□ 96% Aluminum Oxide, Material A, Specimen 2,3
■ 99% Alumina, Material B
▲ 96% Aluminum Oxide, Material A(2)

Refer to Table VI for Specimen Descriptions

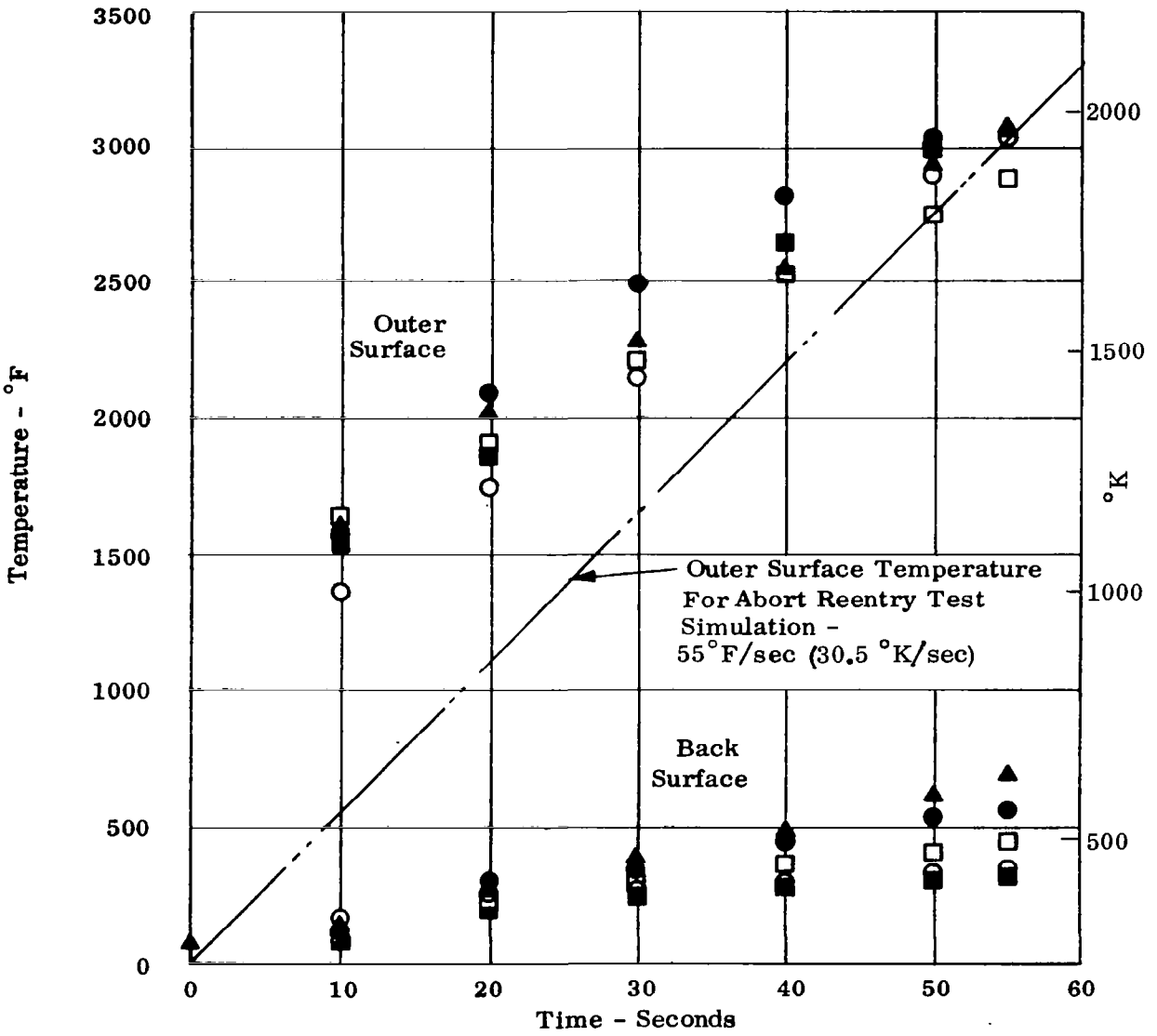

Figure 15. Outer Surface and Back Surface Temperatures versus Heating Time for Ceramic Materials A, B, and F

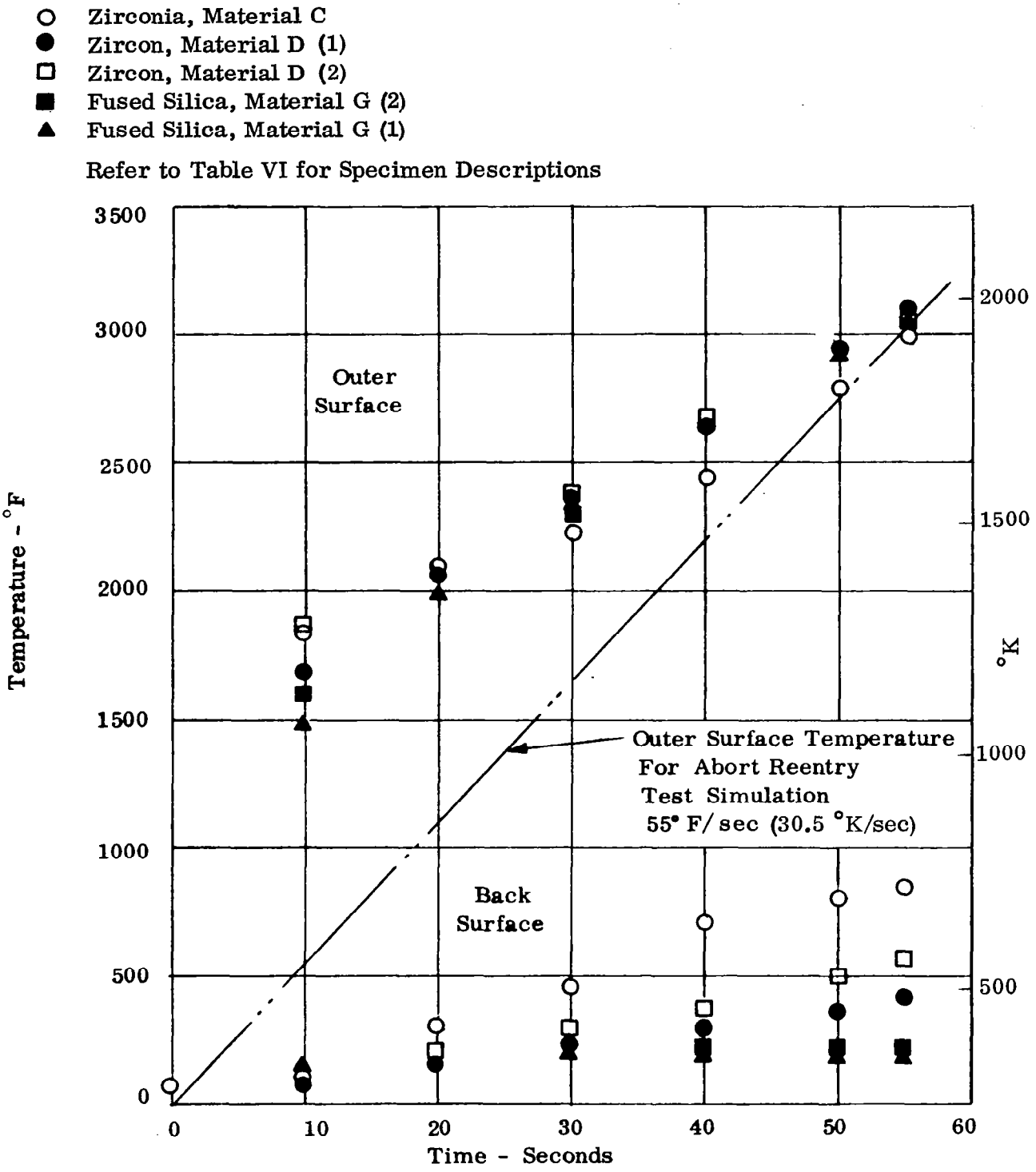

Figure 16. Outer Surface and Back Surface Temperatures versus Heating Time for Ceramic Materials C, D, and G

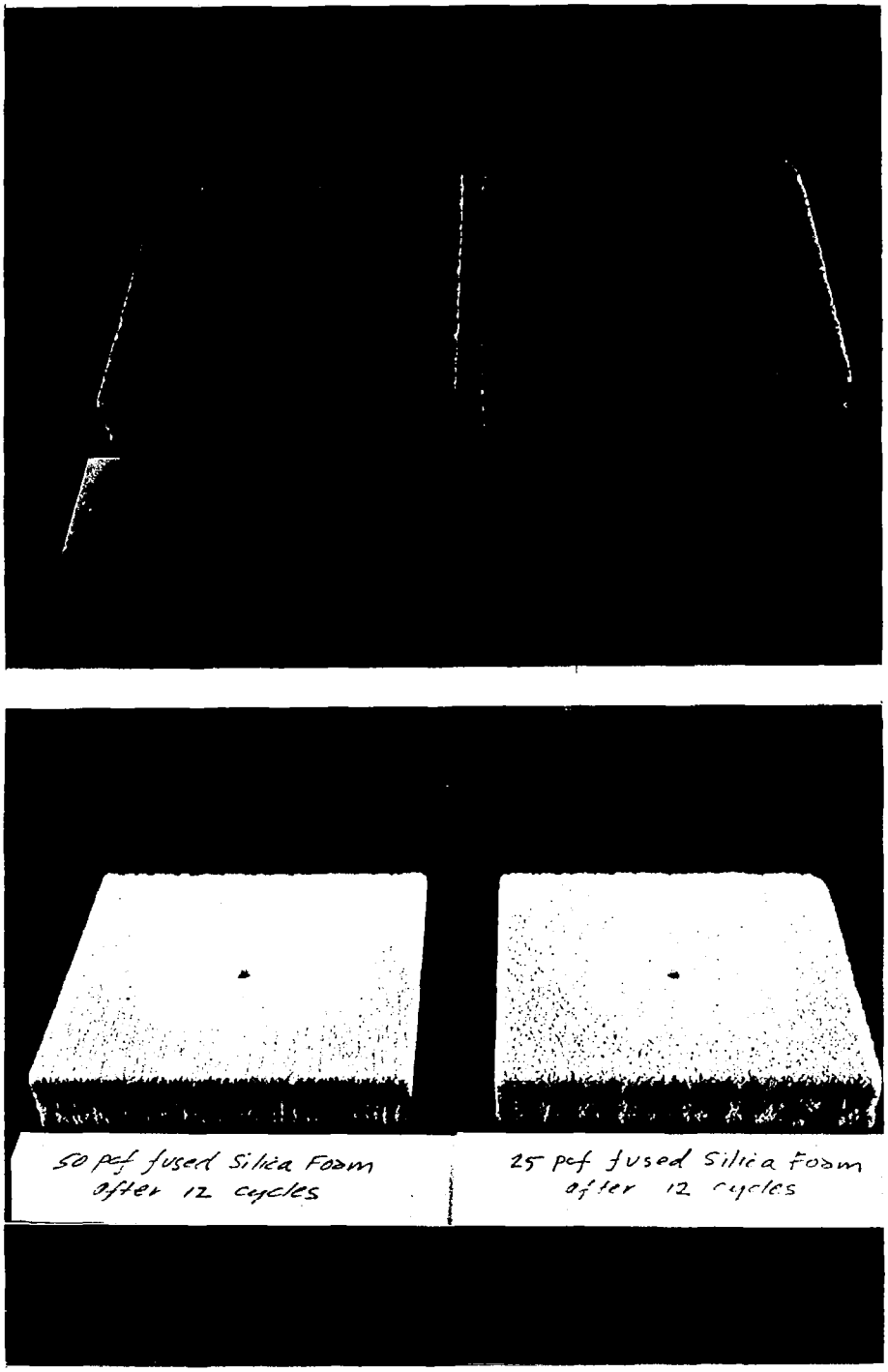

Figure 17. Fused Silica Specimens After 1 and 12 Thermal Shock Tests

TABLE VII TEST AND LITERATURE COMPARISONS OF MODULUS OF RUPTURE AND ELASTICITY AT ROOM TEMPERATURE

		MEASURED MODULUS OF RUPTURE		TENSILE STRENGTH FROM LITERATURE		MODULUS OF ELASTICITY MEASURED		MODULUS OF ELASTICITY LITERATURE	
		lb/m^2	kg/m^2	lb/m^2	kg/m^2	lb/m^2	kg/m^2	lb/m^2	kg/m^2
FUSED	1	146(1)	102 x 10^3	468(3)	(1)328 x 10^3	2.40 x 10^5	1.68x10^8	1.02 x10^5(4)	7.14x10^8
SILICA	2	162	113			2.45	1.71		
25 lb/ft^3	3	145	101			2.49	1.74		
(399 kg/m^3)	4	155	108			1.85	1.29		
	5	152	106			1.90	1.33		
	6	153	106			2.00	1.40		
FUSED	1	294(2)	206 x 10^3	937(3)	(2)655 x 10^3	3.61 x 10^5	2.53x10^8	3.41 x10^5(4)	2.39x10^8
SILICA	2	435	304			4.82	3.37		
50 lb/ft^3	3	365	255			3.79	2.75		
(799 kg/m^3)	4	488	342			5.01	3.51		
	5	453	317			5.72	4.00		
	6	464	325			5.30	3.71		
ALUMINUM SILICATE 50 lb/ft^3 (799 kg/m^3)	1	582	406 x 10^3	425(5)	298 x 10^3	10.7 x 10^5	7.5 x10^8	18.5x 10^5(6)	12.95x10^8
	2	500	500 x 10^3			8.76 x10^5	6.13x10^8		

(1) The MOR DATA indicate a Weibull material constant (m) of about 30. Tensile strength should be about 87% of the Modulus of Rupture for this value of m (Ref. 17).

(2) The MOR DATA indicate an m value of about 6 and tensile shrength should be about 65% of the modulus of rupture (Ref. 17).

(3) Ref. 3 and corrected for porosity according to $\sigma_p = \sigma_o e^{-4p}$

(4) Ref. 4 and corrected for porosity according to $E_p = E_o e^{-6.6p}$

(5) Ref. 5

(6) Ref. 6 and corrected for porosity according to $E = E_o e^{-4p}$

Although the number of tests run were too few in number to be statistically analyzed, a very low degree of scatter was evidenced, especially in the fused silica specimens. Statistical theory is presented in Section V to support the viewpoint that highly porous ceramics would be expected to show small variability in strength of specimens as compared to dense brittle materials.

E. Comparison of Analytical and Experimental Results.

The experimental performances of alumina, aluminum silicate, and zircon were clearly superior to analytical expectations, even considering the differences between the actual properties of the specimens and those used in the analyses. The test performances are interesting in two respects: unusually good thermal shock resistance was demonstrated; and performance repeatability was apparently obtained in specimens of the same material, although the sample size was very small.

With respect to performance repeatability, the parallel structural element concept of Section V should serve as a hypothesis. This should be confirmed with more specimen tests before firm conclusions can be determined. To the extent that this concept applies, the variation of strength should be statistically similar from specimen to specimen, and the performances should be about equal. Also, low strength failures would be localized and specimens of the same material would develop equal overall strength.

It is apparent that the analytical model used in calculating thermal stresses was not completely adequate. This was an elastic plate analysis which assumed an equivalent solid plate corrected for mechanical and thermal property changes due to porosity and temperature. Such a model does not account for certain local strains which may occur in a cellular structure but not in a solid plate, and these strains probably act to reduce thermal stress levels. The analytical model utilized can be considered useful in obtaining relative performances of material or pore geometries, and in this way preliminary designs may be established, which should be confirmed by testing. However, it is necessary to extend the analytical techniques to determine load distribution between cells, and redistribution of load after failure of a number of cells. Such an approach appears achievable, probably through computer analysis of large truss networks to represent the porous constructions. An accurate representation would also provide better insight into the pore geometries required to achieve maximum thermal shock resistance.

IV. HEAT SHIELD DESIGN

It is possible that a single basic heat shield design may prove advantageous in view of the substantial manufacturing quality control and inspection technology associated with each configuration. However, since the load conditions are considerably different in the high and low temperature and pressure sections of the vehicle, there appears to be sufficient justification to investigate separate designs. This section describes the design concepts for the high and low pressure shield areas and describes the principles and approaches used to establish the designs.

A. High Pressure Shields

1. Design Principles

For the heavily loaded heat shield areas, the following design principles are useful:

(a) Provide Minimum Bending Moments in the Ceramic

Relatively high normal pressures during reentry necessitate that the ceramic be supported at short spans, or more desirably, that continuous support be provided at the backface. For effective support, the displacement characteristics of the support elements must assure a more or less uniformly distributed load transfer from the ceramic. Flexible elements such as feltmetals, multiple thin foil elements, honeycombs, etc., can provide uniform support without transmitting high thermal deformation stresses to the ceramic during temperature changes.

(b) Provide Fail Safe Measures

In view of the possibility of meteorite impact or other cause of local damage, it is highly desirable to develop a design which can retain functional capability even after some damage. Fail safe requirements tend to support multiple support of the ceramic modules and use of relatively small modules, each perhaps 1/4 to 1 square foot (0.023 to 0.093 m^2) in surface area. Use of small multiple attachment elements has the further advantage of reducing the possibility of complete failure by crack propagation in the bond interfaces.

(c) Low Attachment Stress in Ceramics

The use of thin foil or small diameter sections at the ceramic metal interface is necessary to assure low restraint of the ceramic. A thick ceramic body will restrain a sufficiently small metal section and cause the deformation of the interface surfaces to nearly correspond to those of a free ceramic body.

2. Configuration for High Pressure Areas

Figure 18 illustrates a design concept which satisfies the above principles to a substantial degree. The support panel consists of a honeycomb core panel with two faces. A layer of feltmetal is the interface between the ceramic and the support panel. The feltmetal provides full support to the ceramic module backfaces. A sufficiently low apparent elastic modulus of the feltmetal assures nearly uniform distribution of ceramic-metal contact pressure, thus avoiding bending moments in the modules.

The ceramic-metal attachment is made up of numerous bonds between the ceramic and the thin wires of the feltmetal. Such an arrangement minimizes the effects of local damage to the ceramic modules or to a portion of the metal-ceramic interface. The attachment is, in effect, a group of parallel flexible connections which, in addition to the multiple bond feature, also support the module without transmitting most of the support panel deflection or deformation loads to the module. With correct sizing of modules, the feltmetal should prevent any significant restraints on the ceramic arising from panel deformation. Moreover, since there is a large choice of wire diameters available, the diameter may be selected appropriately small to assure low thermal stresses at the ceramic interfaces. With small wire diameters, differences in the thermal expansions of the ceramic and metal wires will result in strain of the wires with small local thermal stresses in the ceramic. This is highly desirable, since it is necessary to maintain low ceramic stresses and the metal wires are capable of much larger stresses and strains.

(a) Support Panel Design

Stress analyses of the support panels based on the loads corresponding to the high pressure vehicle surfaces are described in Reference 1. Weight results and material selections from this reference are listed in Table VIII.

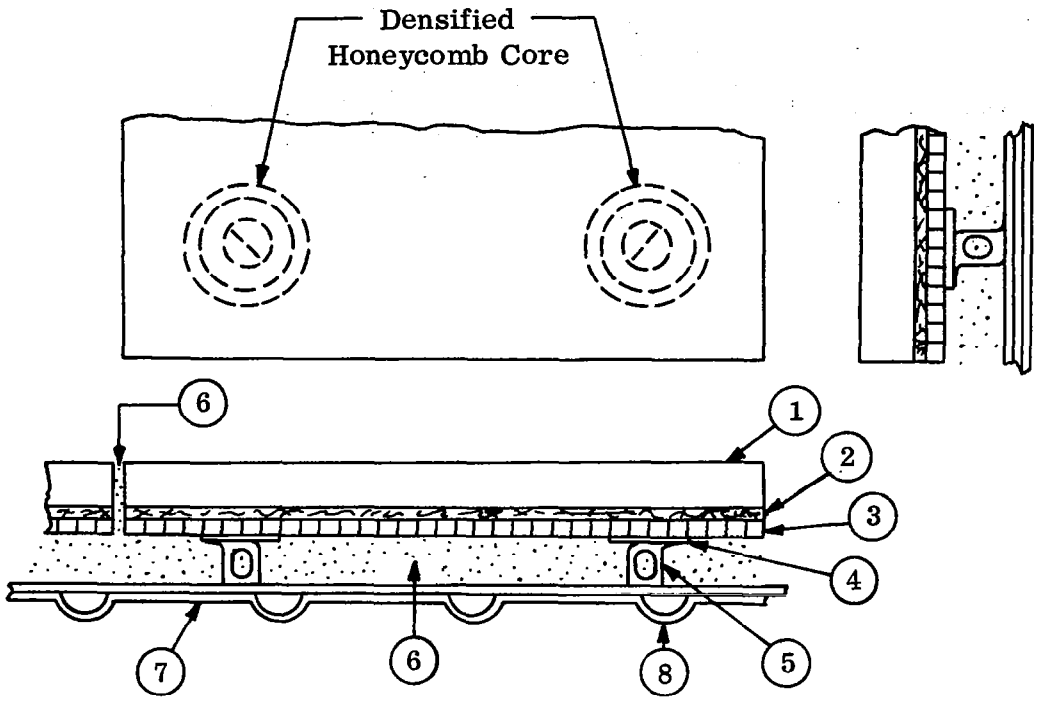

1. Porous Ceramic Module
2. Low Density Feltmetal
3. Honeycomb Sandwich
4. Support Reinforcing Pad
5. Support Leg Attached to Drilled Reinforcing Pad
6. Lightweight Insulation
7. Primary Structure, water cooled
8. Coolant Passages

Figure 18. Ceramic Heat Shield and Support Panel Configuration

The heat shield panels may be made relatively large, 12 x 12 inches (0.3048 x 0.3048 m), or 18 x 18 inches (0.4572 x 0.4572 m), depending on weight and design tradeoffs. The size of ceramic modules may perhaps be limited to 6 x 6 inches (0.1524 x 0.1524 m) as determined by quality or manufacturing capabilities or module-panel restraint considerations. A number of ceramic modules would, therefore, be attached to a single support panel.

Thin metal foil sections, such as channels and honeycombs, may be used in place of the feltmetal. Such designs may have a potential weight reduction as compared to the feltmetal concept, and appear worth investigating. However, these entail a somewhat more difficult design to assure satisfactory stresses and multiplicity of bond surfaces.

TABLE VIII. WEIGHT OF SUPPORT PANELS

	lb/ft^2	kg/m^2
Braze Alloy	0.26	1.26
Feltmetal	0.52	2.53
Two Face Sheets for the Honeycomb Sandwich, .005 inch (0.127 mm) Thick, Hastelloy X	0.43	2.09
Hastelloy Core	0.37	1.80
Support Clips Hastelloy	0.10	0.48
TOTAL	1.68	8.16

(b) Attachment Design

Table IX presents the results of analyses performed, as summarized in Appendix D, to determine suitable materials and dimensions for the ceramic metal interfaces.

In the case of nickel superalloy-alumina combinations, the stresses in the metal are high, beyond the capabilities of the metals if these stresses occur at 1800°F (1250°K). Consequently, it would be necessary to bond at high temperature so that maximum stresses occur at low temperature. Brazing or high temperature ceramic bonding methods are therefore necessary for these material combinations. The stress levels indicated necessitate the use of high strength alloys such as Rene 41.

Silica presents a more difficult problem because of its very low thermal expansion coefficients. Combinations with nickel supperalloys result in excessive stresses in the metal. However, satisfactory stress levels are obtained with Cb alloy D-31. For this, bonding may be at low or high temperature. Cb alloy FS-85 and Ta-10W, however, would be satisfactory only with hot bonding.

The ceramic stresses and the interface shear stresses are low because of the small diameter wire selected. The metal stresses are independent of diameter. Larger metal diameters would increase the ceramic and the shear stresses, and diameters larger than about 0.003 inch would require some densification of the ceramic at the interface. Considering the temperature levels of the attachment area, the limited time at maximum temperatures, and the limited flow of gas to the feltmetal, it is likely that oxidation protection would not be needed for columbium or tantalum wires. However, thin coatings of nickel or silver should greatly increase oxidation protection if necessary.

3. Insulation and Cooling Requirements

(a) X = 2 ft (0.609 m) Vehicle Station, High Pressure Surfaces

One-dimensional transient heat transfer studies were performed to determine optimum ceramic and insulation thickness for the L/D_{max} trajectory. This trajectory provides the longest reentry period and was therefore selected to determine insulation and coolant requirements for the materials which demonstrated promising performance in the thermal shock evaluation tests: alumina, silica, and zircon. The analysis method is presented in Appendix E.

TABLE IX STRESSES ARISING FROM CERAMIC - METAL BONDS UNDERGOING TEMPERATURE CHANGE BETWEEN 70° - 1800°F (294° - 1250°K)

Material Combinations	Wire Diameter		Shear Stress		Stress in Ceramic		Stress in Wire	
	in.	mm	lb/in^2	kg/m^2	lb/in^2	kg/m^2	lb/in^2	kg/m^2
Nickel Superalloy and Alumina	0.002	0.0508	81	56×10^3	64	44×10^3	162,000	113×10^6
Cb Alloy (D-41) and Alumina	0.002	0.0508	6	4.2×10^3	5	3.5×10^3	12,900	9×10^6
Ta (Ta-10W) and Alumina	0.002	0.0508	17	12×10^3	14	9.8×10^3	34,600	24×10^6
Cb Alloy (FS-85) and Silica	0.002	0.0508	54	38×10^3	43	30×10^3	108,900	76×10^6
Cb Alloy (D-31) and Silica	0.002	0.0508	32	22×10^3	26	18×10^3	65,400	46×10^6
Ta Alloy (Ta+10W) and Silica	0.002	0.0508	47	33×10^3	37	26×10^3	93,560	65×10^6

Figure 19 presents the results, as applied for the X = 2 ft (0.609 m) vehicle location. The designs were based on a maximum ceramic-metal interface temperature of about 1800°F, (1250°K) which was considered an acceptable level for the present state of bonding technology. In the case of alumina with 50 lb/ft^3 (799 kg/m^3) density, a thickness of 0.6 inch (0.0152 m) provided a satisfactory balance of ceramic, insulation, and cooling systems weight.

Optimum thicknesses of ceramic were greater for silica and zircon than for alumina. In these cases, the lower ceramic density, 25 lb/ft^3 (399 kg/m^3), enables efficient use of thick ceramic and insulation sections with consequent large reductions in the cooling system requirements.

The results of Figure 19 are based on a water-cooling system with 1,000 BTU/lb (1.055 x 10^6 J/kg) latent heat. The weight of the coolant system was assumed to be equal to one-half of the weight of the coolant. Also, the total average heat transfer to the cooling system, per unit area, at X = 2 ft (0.609 m) was approximated as one-half of that occurring at the lower center line at the same vehicle station.

(b) X = 6 ft (1.828 m) Location, Below Horizontal Centerlines, High Pressure Surfaces

Figure 20 presents similar studies for the X = 6 ft (1.828 m) location. Because of the lower surface heat inputs, a larger proportion of lightweight insulation can be applied, thus lowering coolant needs and overall weight. The data in Figure 22 were developed with the same premises used for Figure 19.

4. Weight Summary

Lowest estimate weights for heat shield panels applicable to the high pressure vehicle surfaces are summarized in Table X.

B. Configurations for Low Pressure Shield Areas

The pressure loads are sufficiently low at the surfaces above the horizontal centerlines aft of X = 4 ft (1.22 m), that four-point supports may be considered for the ceramic modules rather than the full support panel design used for the high pressure shields.

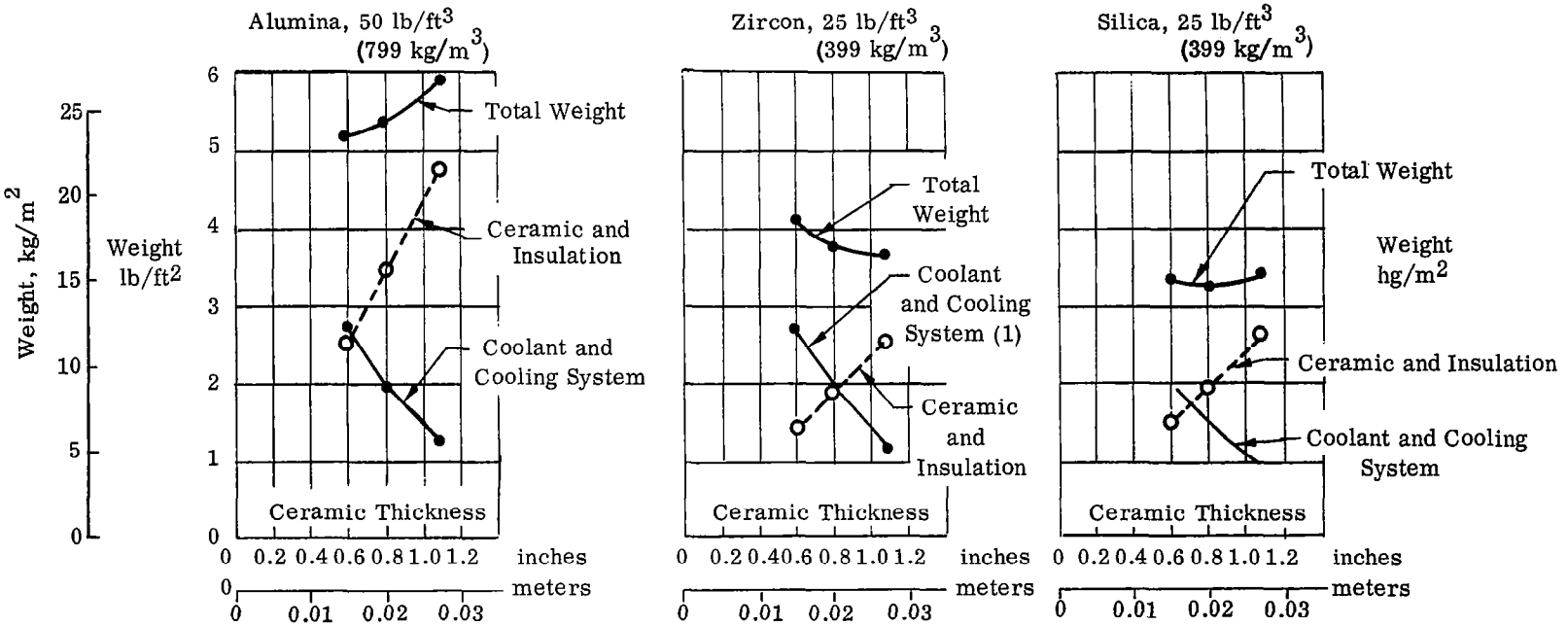

Minimum Weight Systems	Alumina	Zircon	Silica
(a) Ceramic Thickness	0.6 in. (0.015 m)	1.1 (0.028 m)	0.8 in. (0.020 m)
(b) Insulation Thickness Dynaquartz	0.15 in. (0.0038 m)	0.3 in. (0.0076 m)	0.3 in. (0.0076 m)
(c) Total Average Heat Transfer to Cooling System at X = 2 ft (0.609 m) During Reentry	1745 BTU/ft^2 1979 x 10^4 J/m^2)	795 BTU/ft^2 902 x 10^4 J/m^2	950 BTU/ft^2 1077 x 10^4 J/m^2

Figure 19. Insulation and Cooling System Weights for L/D_{max} Reentry at X = 2 ft (0.609 m)

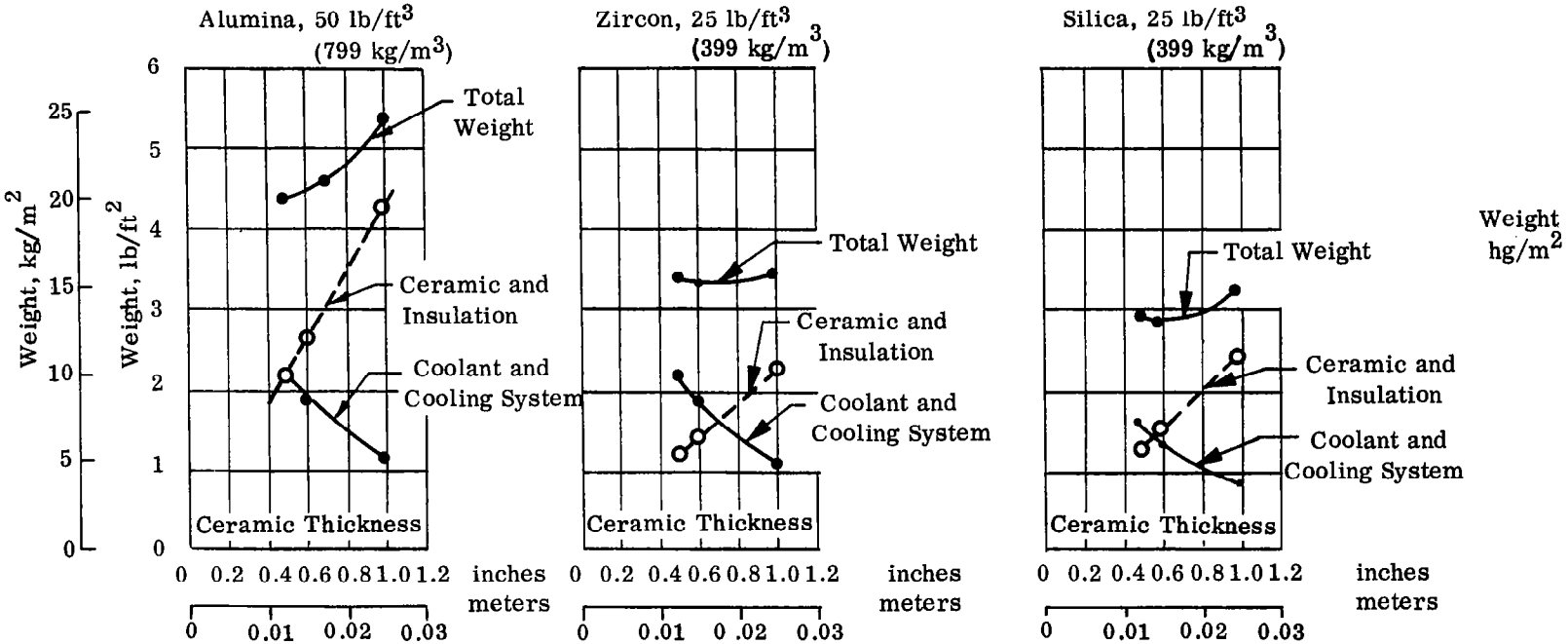

Minimum Weight Systems	Alumina	Zircon	Silica
(a) Ceramic Thickness	0.5 in. (0.0127 m)	0.6 in. (0.015 m)	0.6 in. (0.015 m)
(b) Insulation Thickness	0.25 in. (0.0063 m)	0.3 in. (0.0076 m)	0.4 in. (0.010 m)
(c) Total Average Heat Transfer to Cooling System at X - 6 ft (1.8 m) During Reentry	1000 BTU/ft^2 1134 x 10^4 J/m^2	825 BTU/ft^2 936 x 10^4 J/m^2	620 BTU/ft^2 703 x 10^4 J/m^2

Figure 20. Insulation and Cooling System Weights for L/D_{max} Reentry at X = 6 ft (1.828 m)

TABLE X HEAT SHIELD WEIGHT FOR HIGH PRESSURE VEHICLE SURFACES

Heat Shield Materials	Support Panel Weight lb/ft^2	kg/m^2	Ceramic Insulation Coolant and Coolant System Weight lb/ft^2	kg/m^2	Total Weight lb/ft^2	kg/m^2
Location X=2 ft (0.609m)						
Alumina	1.68	8.18	5.18	25.25	6.86	33.40
Silica	1.68	8.18	3.26	15.85	4.94	24.05
Zircon	1.68	8.18	3.69	17.95	5.37	26.15
Location X=6 ft (1.828m)						
Alumina	1.68	8.18	4.40	21.40	6.08	29.60
Silica	1.68	8.18	2.90	14.10	4.58	17.40
Zircon	1.68	8.18	3.31	16.10	4.99	24.30

The bending loads must be low enough, compared to the material strength, to assure high reliability design approaches. Nevertheless, the multiplicity of support elements and fail-safe features would be sacrificed to some degree.

The design of four-point supports is critical and must be based on the same principle applied to the high pressure shields; i.e., the metal elements connecting to the ceramic must have low stiffness so that the ceramic strains and stresses are small.

1. Concepts

An attachment for the low pressure region is presented in Figure 21, showing a feltmetal pad as the connecting element between the ceramic module and a sheet metal clip which joins to the primary structure. The spaces between the module and the primary structure, and between the edges of adjacent modules are filled with lightweight fibrous insulation such as Dynaquartz.

2. Weight Summary

Reference 1 presents the results of stress studies which indicate that the 4-point supported modules of fused silica must have a thickness of 1/2 inch (0.0127 m) if the density of the silica is 68.5 lb/ft^3 (1092 kg/m^3), or 1 inch (0.0254 m) if the density is reduced to half of the above value. The weight of the ceramic module becomes 2.85 lb/ft^2 (13.9 kg/m^2) in either case. The lower density ceramic has a greater insulation effect, however, and therefore provides a lower overall shield weight.

Considering the weight of the fibrous insulation, attachment clips, and cooling provisions, the system weight averages 3.70 lb/ft^2 (18.0 kg/m^2) in the low pressure vehicle region using one foot square (0.093 m^2) fused silica modules supported at four points. The optimum thickness of insulation depends on the local temperature conditions. Optimum weights, given in Table XI, were determined by holding the ceramic module thickness at one inch (0.0254 m) because of structural requirements and varying the thickness of insulation until a minimum weight of insulation and cooling system was obtained.

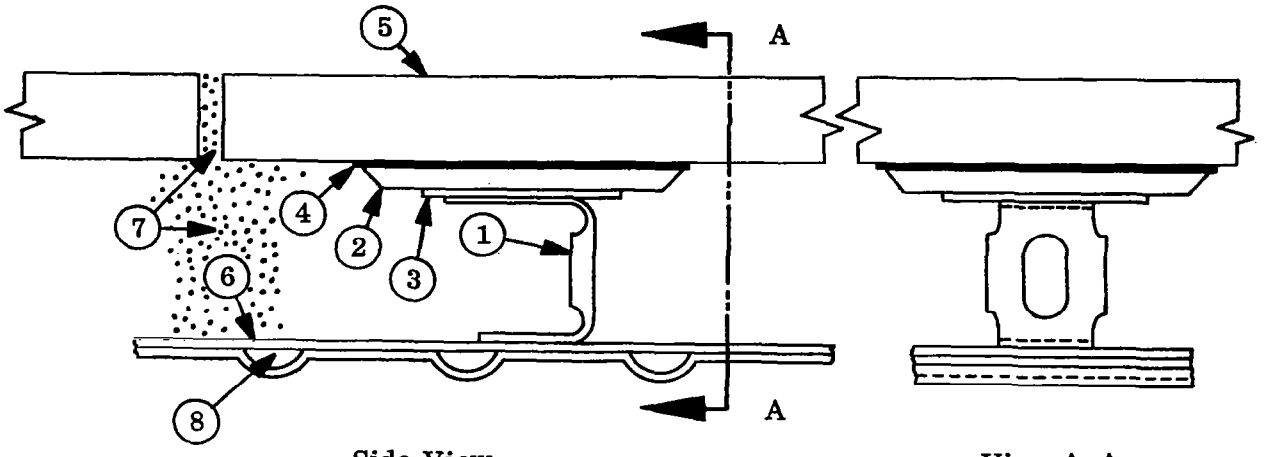

(1) Sheet Metal Clip Weld to (3) and Braze Assembly to (2)

(2) Sintered Fiber Feltmetal Pad

(3) Sheet Metal Reinforcing Disc

(4) Cemented Bond Feltmetal to Element (5)

(5) Rigid or Brittle Element to be Supported

(6) Primary Structure

(7) Lightweight Insulation

(8) Coolant Passages

Figure 21. Attachment Design for Low Pressure Region

TABLE XI. SHIELD WEIGHTS FOR FOUR-POINT SUPPORTED CERAMIC DESIGN

Outside Surface Temperature	2400°F (1585°K)	1800°F (1255°K)
Insulation Thickness	0.80 inch (0.0201 m)	0.60 inch (0.0151 m)
WEIGHTS	lb/ft^2, (kg/m^2)	lb/ft^2, (kg/m^2)
Insulation Weight	0.33 (1.61)	0.24 (1.17)
Ceramic Module Weight	2.85 (13.90)	2.85 (13.90)
Coolant and Cooling System Weight	0.49 (2.39)	0.45 (2.20)
Attachments	0.10 (0.49)	0.10 (0.49)
TOTAL WEIGHT	3.77 lb/ft^2 (18.41 kg/m^2)	3.64 lb/ft^2 (17.78 kg/m^2)

The concepts used for the high pressure shields are also competitive for the low pressure regions. Use of a support panel permits application of a lower density ceramic which offsets the weight of the support panel. With a ceramic module of silica of 25 lb/ft^3 (399 kg/m^3) density and 0.55 inch (0.0140 m) thickness, a design similar to Figure 18 but applicable to the low pressure vehicle sections has a total weight of 3.85 lb/ft^2 (18.74 kg/m^2), as described in Table XII.

TABLE XII. SHIELD WEIGHTS FOR FULLY SUPPORTED CERAMIC DESIGN

	lb/ft^2	kg/m^2
Ceramic	1.14	5.56
Support Panel	1.68	8.16
Insulation Thickness 0.55 inch (0.0140 m)	0.23	1.12
Cooling System and Coolant	0.80	3.90
TOTAL	3.85	18.74

A choice exists in the selection of heat shield design between 4-point attachments and fully supported modules. Since the weights of these concepts are about equal, final selection would depend on more detailed studies of the characteristics of available materials and the requirements of the vehicle.

C. Vibration Characteristics

The dynamic response of the ceramic modules, when supported by feltmetal, is calculated in Reference 1. It is shown that dynamic responses are very small at the levels indicated by Figure 9. The dynamic characteristics are affected by the feltmetal density, and it appears possible to alter vibration response to obtain desired performance for given environments.

D. Removal and Installation of Heat Shield Panels from the Exterior

Removal and installation of heat shield panels from the exterior of the vehicle may be an important advantage during vehicle assembly and also during preparation for an additional flight. This would avoid extensive vehicle disassembly in the event certain critically located panels were damaged and had to be replaced. Appendix D presents attachment concepts which would permit removal and installation of panels from the exterior of the vehicle.

V. STATISTICAL STUDIES OF BRITTLE STRUCTURES

An understanding of the variability effects in the highly porous constructions studied in this program is important. The thermal shock tests indicated a rather good consistency, in that all specimens of such material seem to perform similarly. Also, the modulus of rupture tests showed rather small variations. However, the number of specimens was very small and recourse to statistical theory was made to obtain a better insight into the response of the materials.

Test observations, however, seemed to indicate that conventional statistical approaches for brittle materials were not realistic for the porous materials tested. The modules did not appear sensitive to notches during thermal stress testing. Roughly drilled thermocouple holes through the specimens did not act as crack initiation sites. Surface cuts, made to relieve thermal stresses, also showed no evidence of inducing cracks. Further, the bend specimens were cut roughly because adequate cutting techniques for porous specimens were lacking, and yet the rupture stresses were remarkably uniform.

Most previous statistical work has considered that the brittle body acts as a chain of links in series. The fractured one link will cause failure of the whole body. Thus, the body operates as a series structure and the weakest element determines the strength of the body. Such a series model appears to well represent solid structural components made of brittle material. The strength of each structural element is influenced by the microscopic cracks and flaws, which will propagate through adjacent material when sufficient energy is applied. The tips of the propagated cracks are always very sharp, thus concentrating stress and energy and inducing a tendency to crack rapidly. Cracks propagating from the weakest material areas can therefore destroy the entire structural element.

Highly porous ceramic materials appear to have modified load distribution and failure characteristics. First, the porous structure contains parallel loading paths. If a portion of the structure fails, load can be redistributed and the body may continue to function. Secondly, crack propagation is inhibited as each crack leads to a pore of finite diameter. The much larger diameter of the pore will make crack propagation more difficult. On an intuitive basis, it appears that the drastic weakening effect of flaws will be limited to the individual cell walls, and as the weakest walls break, the load level is increased on the adjacent walls.

Using this concept of load distribution, together with the apparent limitations in the extent of crack propagation possible, it is speculated that a parallel structure model could exhibit certain desirable features unusual to brittle materials. Progressive cracking of the weak walls would transfer the load to the stronger ones. In the usual strength distributions of brittle materials, however, relatively few specimens have low strength while a large number of specimens are close to the mean strength. Loss of the weakest elements apparently, therefore, would not necessarily reduce the load carrying capabilities of the structure to a great extent. After the weak elements have failed, the structure should remain stable. Definition of the load levels that can be resisted in a parallel structure is, therefore, important. The analysis in this section determines the statistical relationships defining the load levels and the number of failed elements. The analysis shows that even for a highly variable material, the maximum load which could be carried by the parallel structure occurs when 39% of the fibers have broken. The corresponding stress level of the remaining fibers is therefore close to the mean strength of the material. If the parallel structure consists of many elements, all parallel structure specimens would be expected to have a similar strength distribution in their elements. Further, the specimens would be expected to be essentially equal. While the element strength variation would be high, the variation of strength between parallel structure specimens would be small. Consequently, relatively high design stresses as indicated by Figure 22 appear feasible for consideration. With higher values of m, obtained by improved material fabrication, the maximum loading will increase.

Whether a parallel model accurately represents the lacy-type construction, of course, is not known. In a sense, the parallel model is too severe a representation. A break in one of the fibers of a purely parallel model will reduce the strength along the entire bundle length. In the lacy construction, the effect of a break in a single cell wall would be felt over a limited length because of cell interconnections in three dimensions.

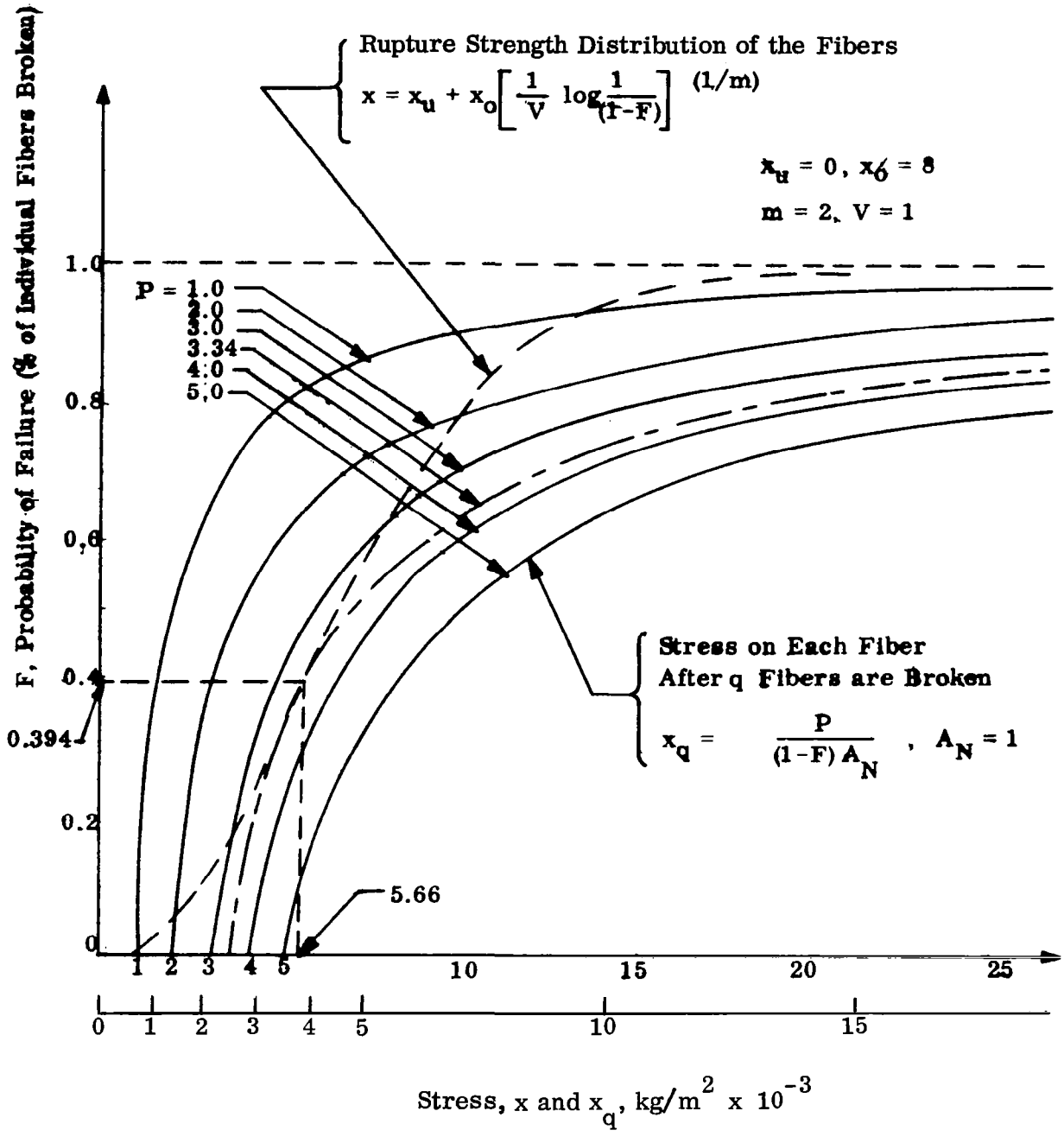

Figure 22. Interrelationship of Stress on Each Fiber and Strength Distribution of Fibers

A. Load and Element Failure Relationships

Consider a bundle of parallel fibrous structures subjected to a constant tensile load, P. The tensile stress on each element or fiber will be,

$$(x)_o = \frac{P}{NA} = \frac{P}{A_N} \tag{1}$$

where

A = Cross-sectional area of each fiber

A_N = Total cross-sectional area

N = Number of fibers

$(x)_o$ = Tensile stress on each fiber when no fiber has been broken

When q fibers have been broken, the tensile stress on each fiber will be,

$$x_q = \frac{P}{(N - q)\,A} = \frac{P}{r\,A} = \frac{P}{A_r} \tag{2}$$

$$N - q = r$$

where

r = Number of remaining fibers

A_r = Cross-sectional area of the remaining fibers

The probability of failure among the fibers will be,

$$F = \frac{q}{N} \tag{3}$$

Combining Equations (2) and (4)

$$x_q = \frac{P}{\left[1 - \frac{q}{N}\right] NA} = \frac{P}{(1 - F) A_N} \qquad (5)$$

Recall Weibull's distribution function of probability of failure

$$\begin{cases} F(x) = 1 - \exp\left[-V \dfrac{x - x_u}{x_o}\right]^m & (x \geq x_u) \\ F(x) = 1 - \exp(o) - 1 - 1 = o & (x < x_u) \end{cases} \qquad (6)$$

Rearranging the above equation

$$x - x_u + x_o \left[\frac{1 \log}{V} \frac{1}{(1 - F)}\right]^{1/m} \qquad (7)$$

where

x = Rupture strength distribution

x_u = Threshold stress

x_o = Material characteristic stress

m = Material variability

Equations (5) and (7) are plotted in Figure 22. These two functions are different in nature. They cross each other at various locations depending upon the magnitude of the external load P and the Weibull constants of the material, x_o, x_u, and m. Note from Figure 22 that the number of fibers which would rupture is limited for loads $P \leq 3.34$. At $P = 3.34$, 39.5% of the fibers are broken. With further load the fibers would rupture to complete failure.

VI. MANUFACTURING AND INSPECTION CONSIDERATIONS

The most important single question regarding manufacturing of porous ceramics is whether sufficient quality control can be achieved within a reasonable time to support a heat shield project requirement. The various methods of constructing porous bodies are well known but means of achieving a high degree of reproducibility are relatively unexplored.

Based on the studies of this program, a high degree of quality control is believed attainable with moderate expenditures through a systematic effort designed to instrument, control, and establish optimum process operations. Because the variations in certain process operations have large effects on the product, a high degree of process control is an anticipated requirement, comparable to that applied to many sophisticated chemical processes. The development of a high standard of material quality should be scheduled early in any heat shield development program to avoid the possibility of testing hardware subject to manufacturing errors.

A. Process Quality Control

Effective quality control procedures can be based on a knowledge of the functions of the components of the system as well as an understanding of the effects of certain process variations. Regarding the components of a urethane system, knowledge of the prepolymer, stabilizers, and catalyst are important, since these influence the film properties of the resin. Instability of the film leads to uneven expansion with resulting nonuniform structure. Process variables are important in that structural uniformity and integrity are influenced by relatively small changes in the physical parameters. This is appreciated when it is considered that gas evolution is the primary means of controlling the degree of porosity. The pore geometry, moreover, is dependent upon the viscosity and surface tension of the resin film. The process essentially involves the expansion of a mix of liquid organics and ceramic powders.

Nevertheless, laboratory experience indicates that consistent ceramic specimens can be repeatedly achieved. In addition, indications are that processing can be scaled up to a manufacturing level, providing adequate control is applied to the parameters identified in the laboratory work. At least one of the material suppliers used in this program appears to have already demonstrated consistent construction of experimental specimens, indicating a good grasp of the control parameters. Since the specimens were made through

variations of standard manufacturing processes to obtain certain density and porosity changes, the modified processes are believed to be readily applicable to production operations. Whether sufficient controls are being applied to obtain the uniformity desired for flight vehicles, however, is not known. In all probability, additional controls would have to be developed to assure a low specimen rejection rate.

Other material suppliers have experienced considerable difficulty in reproducing specific foam geometries. A good part of the problem seems to be caused by inadequate knowledge of the foaming reactions, lack of precise documentation of the process, and insufficient control of the raw materials and process conditions. The controlling independent variables in the preparation of a polyurethane foam with ceramic fill are listed and discussed in Reference 1, Section 7.

B. Inspection and Reusability

Inspection methods are necessary to evaluate the process or batch, the as-received components, and the components to be reused. The work of this program with respect to inspection was carried to the point of indicating the potential usefulness of several inspection methods. In all cases, considerable additional inspection study effort is needed to permit effective use of any of the inspection methods described in this section. It appears that, although the basic inspection techniques are available to adequately evaluate the materials, extensive inspection data must be derived to define the state of specimens in question.

1. As-received Product - Inspection of a Small Sampling to Evaluate the Batch

The following tests are useful in evaluating the processing composition and the properties of the batch of ceramic modules:

a. Microscopic inspection at various magnifications to characterize microstructure, pore size distribution, cell wall structure, cracks, damage, etc. Ultimately, acceptance standards can be developed.

b. Phase Identification - X-ray diffraction studies provide a means of identifying the material phases and thereby enable a check with respect to such factors as raw material composition and the process conditions which affect the material phases in the final product.

c. Mechanical Test - Elastic modulus and modulus of rupture properties strongly affect the thermal shock resistance of a material and are, therefore, logical inspection tests. Acceptable variations may be defined for individual materials based on test observation and giving consideration to analytical studies of the effects of these properties on the thermal shock resistance of the materials.

2. As-received Product - Selection Tests

Thermal shock testing appears ideally suited as a proof selection test procedure because it combines mechanical, thermal, and chemical effects. Purely mechanical tests such as modulus of rupture and compression tests are also valuable and are generally more easily interpreted. However, with an accurate heating test apparatus and with reference to thermal stress analyses, a simple thermal test can be planned to effectively evaluate a component. The initial proof test will have to be designed according to the endurance and damage criteria, as discussed below.

3. Inspection and Reusability

Damage criteria must be established to enable evaluation of a part for reuse. This involves repetitive testing and inspection of specimens which have been selected on the basis of an initial proof test to eliminate all weak specimens.

The damage criteria developed on the basis of repetitive testing may include a variety of inspections. X-ray diffraction studies may be conducted to determine phase changes. The x-ray diffraction studies of fused silica before and after test (as performed in the course of this program) may be extended to establish acceptable limits for cristobolite formation. Similarly, mechanical testing may be applied to evaluate changes in the components after a period of use.

The inspections previously suggested to determine reusability are essentially destructive in nature. However, since the vehicle would contain many ceramic modules, it is practical to select a representative sampling of modules from the most severely stressed section of the vehicle to provide an evaluation of the entire heat shield. Thermal shock tests may also be applied to selected modules to provide a direct determination of the cycle life remaining in the heat shield.

Nondestructive tests should also be applied to sections or perhaps the entire heat shield. These include visual inspections, application of pressure loads (together with simple strain measurements), and shake tests.

VII. COMPARISON OF POROUS CERAMIC AND ABLATIVE HEAT SHIELDS

Approximate comparisons can be developed for porous ceramic radiation shields and ablative shields for application for a lifting body vehicle. A considerable degree of uncertainty exists with either approach with respect to weight, cost, and reliability, because adequate performance testing has not been conducted to evaluate the materials under the lifting vehicle environments.

To achieve reasonable ablative weight properties, it is necessary to be able to accurately predict local environmental thermal inputs and also the temperature distributions through the ablator, the substrate panel, and the bonding surface. The ablative shield weight is temperature-sensitive in that any uncertainty with respect to local thermal conditions must be compensated by an increase in the local thickness of the ablator. Considering the variety of possible flight conditions, and decreases in accuracy, both in the knowledge of local flow fields and heat transfer characteristics as distance from the stagnation area increases, the added weight needed to compensate for thermal uncertainty may be appreciable.

If sufficient surface roughness or discontinuities develop as a result of weakness in the surface char, to cause flow separation, the thermal inputs at the boundary layer reattachment area will be substantially higher.

Material manufacturing variation and ablation characteristics have a bearing on weight and must be considered in establishing the ablator thickness for lifting body reentry involving a long period of time. Variations in ablator thermal conductivity, density, and transpiration factors significantly influence bond line temperature.

The weight of porous ceramic shields is not as sensitive to variations in local heating conditions, since the cooling system is able to average the heat load. A thermal capacity safety factor may be applied through a small increase in the amount of coolant available; this added capacity could be utilized at any local region subjected to unexpectedly high total thermal input. However, a sustained local outer surface temperature considerably above the design value could cause excessive temperature at the ceramic-metal interface. But since maximum temperatures are of short duration, the thermal lags in the material may be sufficient to offset any problems at the interface, or require at most, a small increase in the thickness of the ceramic.

Reference 7 indicates an overall ablative shield system of 4 lb/ft^2 (19.5 kg/m^2), while an approximate average weight for the high and low pressure regions of the ceramic shield is 4.2 lb/ft^2 (20.5 kg/m^2). It is, of course, not known to what extent more detailed considerations, such as those already mentioned, or test experience would modify the above values. Another significant weight factor may be in the heat load transmitted to the interior of the vehicle, thereby requiring an increase in the internal environmental equipment. The ceramic concepts are based on sufficiently cold water walls, not exceeding 100 °F (310 °K), so that essentially no internal conditioning capacity need be allocated for absorption of heat through the heat shield.

The ceramic shield materials would appear to be more susceptible to thermal stress damage than ablators, if the local temperature rise rates are greater than expected. This would not necessarily create a design weight disadvantage but may certainly be a reliability factor. As a compensating approach, a safety margin may be included in the temperature rise rates. Increased design knowledge, such as a better understanding of thermal stress development in porous materials, and accurate assessment of stress relieving techniques, such as surface cutting, will greatly reduce or eliminate this reliability disadvantage.

In the event of local failure of the heat shield layer material, the ablative designs would appear to be more susceptible to catastrophic failure because the temperature capabilities of the substrate panels and the uncooled structure would be extremely limited. The superalloy support panels in the ceramic shields would offer resistance to all but the hottest portions of the reentry and perhaps permit sufficient time to undertake emergency procedures. Moreover, the water cooled structure would tend to maintain structural integrity until depletion of the coolant.

Cost estimates are presented in Reference 7 in some detail and the outlook is for a cost of about $\$700/ft^2$ ($\$7525/m^2$) for the heat shield panels, including the ablator, substrate panels, insulation materials, and attachments.

A very approximate cost for the ceramic shields is shown in Table XIII, equal to $\$395/ft^2$ ($\$4251/m^2$), plus an additional $\$200/ft^2$ ($\$2150/m^2$) for the cooling system.

TABLE XIII COST OF CERAMIC HEAT SHIELD

	MATERIALS		LABOR		TOTAL	
	$/ft^2	$/m^2	$/ft^2	$/m^2	$/ft^2	$/m^2
Feltmetal (Superalloy)(1)	50	537	25	269	75	807
Honeycomb Support Panel (Hastelloy X)	100	1075	100(2)	1075	200	2150
Attachment Clips	5	54	5	54	10	108
Ceramic	25	269			25	269
Ceramic Bonding			25	269	25	269
Insulation	5	54	5	54	10	108
Quality Inspection			50	540	50	540
Heat Shield Totals	185	1989	210	2261	395	4251
Cooling System					200	2150
			Totals		$595/ft^2	$6401/m^2

Notes:

(1) If a refractory metal feltmetal is required, it is estimated that overall material costs will increase $100/ft^2 ($1075/m^2)

(2) Includes brazing of sandwich panel, feltmetal, and support clips.

Each successive flight may require inspection and refurbishment cost equal to 10% of the heat shield. The cost outlook for repetitive use of the vehicle is listed in Table XIV.

TABLE XIV. COST PREDICTION FOR REPETITIVE USES OF CERAMIC SHIELDS

	Cost of Heat Shield and Cooling System	
One Flight	$595/ft^2	$6401/m^2
Two Flights	$327/ft^2	$3515/m^2
Five Flights	$167/ft^2	$1795/m^2
Ten Flights	$113/ft^2	$1215/m^2

VIII. CONCLUSIONS

The studies presented in this report indicate promise for the application of ceramic heat shields to manned reentry vehicles. It is nevertheless apparent that realization of the benefits of highly refractory and stable heat shields requires further refinement of structural analyses and material technologies. These additional efforts appear within the realm of achievement, however, and can be accomplished in time to support the lift body vehicle projects of the future. The discussion below summarizes the significant conclusions of the study and identifies necessary future effort.

A. Feasibility of Using Ceramics

The test observations and the statistical studies suggest that the highly porous materials are far less sensitive to notches, flaws, or other damage than solid ceramics. The porous construction appears to act as a multi-component structural system capable of redistributing load if some of the elements fail. Further, the existence of numerous pores inhibits crack propogations. Although considerable additional work is needed to characterize the performance of porous ceramics, the ability of the test specimens to survive repeated thermal shock (despite the existence of roughly drilled holes, surface cuts, and general surface roughness) demonstrates feasibility for heat shield use and also indicates that the severe fracture problems associated with dense brittle materials may be significantly alleviated.

B. Design Configuration Evaluation

The designs developed in the course of this program appear attractive from a weight standpoint and also in regard to component simplicity and replaceability. The mechanical design seems relatively straightforward in that the function of each component is well defined. However, while an attempt has been made to provide a better understanding of the stresses involved in rapid heating of porous ceramics, more work is needed to provide an adequate mathematical model. If an adequate model can be developed (and there is every reason to believe that this is possible), the selection of ceramic modules can be based on fundamental factors as well as test experience, with a consequent increase in confidence. Moreover, improved porous configurations may be derived analytically much more readily than through trial testing.

It is believed that the attachment principles described in this report will help establish more rational attachment designs and avoid basic errors often introduced in constructing metal-ceramic joints. The analyses presented indicate the sensitivity of bond systems to material properties, geometry, and thickness of the metal components. However, systems can be designed on the premise that ceramic stresses in the bond regions must be low. The use of felt-metal or thin metallic elements at the interface allows proportioning of metal and ceramic stresses to desired levels. The proposed designs should be evaluated by test.

C. Materials Quality and Processing Outlook

The promising performance of several materials tested in this program should be interpreted as a confirmation of the feasibility of using such materials for heat shield use. Development effort is needed, however, to improve the material properties and to achieve quality control. Perhaps the single most important task required is the improvement of the materials through documentation of current laboratory procedures, study of the effects of the primary process variables, and determination of optimum process conditions. This may be achieved with reasonable time and effort through a systematic study.

D. Weight Outlook

The weight determinations presented in Section IV are attractive and are comparable to nominal weight estimates of ablative systems for similar vehicles. It must be considered that the weight estimates presented for the ceramic concepts include an internal cooling system, and that an accurate comparison of ablative and ceramic radiative shields should consider differences in structural weights and cabin environmental systems.

In all probability, the differences in overall weight of ablative and ceramic systems will be relatively small, and may ultimately favor ceramic shields after a state of development comparable to that already achieved for ablative materials. Choice will most likely hinge on other factors, i.e., ability to reuse vehicle, cost, flexibility in mission, reliability, and other factors.

E. Vehicle Design Factors

The substantial potential advantages of ceramics (reusability, high temperature resistance which enables stable vehicle contours throughout the reentry, low cost, etc.) must be supplemented with an improved reliability outlook. As already suggested, increased processing knowledge, better analytical evaluation techniques, and more test experience would increase confidence and reliability.

Functional capability, however, is substantially enhanced by certain design features. For example, multiple bond elements between the ceramic module and the support panel will tend to prevent catastrophic failures of the attachment. Further, the support panels can offer appreciable protection during a large portion of the reentry flight in the event of failure of the ceramic modules. Also, higher-than-expected local heat inputs could be compensated by coolant flow adjustments. A relatively large increase in local coolant capacity may be provided by a small increase in the total coolant quantity. Such design features provide a degree of operational flexibility necessary to a flight system intended for long-duration reentry flights.

F. Cost

The initial cost of a ceramic heat shield system is comparable to that of an ablative system. However, the economy of the ceramic shield increases rapidly with repeated flights.

G. Recommended Future Work

The most logical areas of future work are those relating to basic technologies which must be developed to permit rational structural and material design approaches to the application of porous ceramics to vehicles. To the extent that these technologies are deficient, the amount of trial testing would have to be increased to demonstrate reliability in any future application. The items listed below are appropriate to an early achievement of a sufficient technology to enable a sound approach to vehicle heat shield applications:

(1) Develop mathematical models to represent structurally porous ceramic constructions. The analytical representations should define: (a) effects of local strains (particularly with respect to possible relief of thermal stresses); (b) load transfer characteristics between cells; (c) the degree to which various pore geometries act as series or parallel structural elements.

(2) Evaluate the analytical models experimentally by mechanical tests of selected pore geometries.

(3) Systematically investigate the process variables for several of the most promising ceramic materials and determine optimum process techniques. Document the process and define the required process measurements to assure quality control.

(4) Using the knowledge of items (1) through (3), construct a series of test specimens, and perform mechanical and thermal tests to obtain representative statistical determinations of material properties.

(5) Develop bonding systems for the promising ceramic and metal combinations. Define the bonding process adequately to enable quality control. Construct test specimens and determine mechanical properties of the attachments.

REFERENCES

1 KRUSOS, J. N., "A Study of Thermal Protection Systems Based on Porous Ceramic Designs for Application to Manned Lifting Reentry Vehicles," Bell Aerosystems Co. Report No. 2296-941012, February 1967.

2 ANTHONY, F. M., HUFF, R. D., "Analytical Evaluation of Actively Cooled Modified Monocoque Structural Sandwich Concepts," AFFDL-TR-65-124, July 1965.

3 FRICKE, W. and SQUIRE, W., "External Noise Fields of a Boost-Glide Hypersonic Vehicle," 28th Symposium on Shock, Vibration and Associated Environments, Washington D.C., February 9, 1960.

4 ELIASON, L. K. and ZOLLNER, G. C., "A Survey of High Temperature Ceramic Materials for Radomes, ML-TDR-64-296, September 1964.

5 Corning Glass Technical Data Sheets, Section 5, Material No. 6941, April 9, 1963.

6 Technical Data (Greenlite -30), A. P. Green Firebrick Co. May 24, 1965.

7 "Refractory Ceramics of Interest in Aerospace Structural Applications - A Materials Selection Handbook," RTD-TDR-63-4102, October 1963.

8 LaPORTE, A. H., "Research on Refurbishable Thermo-structural Panels for Manned Lifting Entry Vehicles, Contract NAS 1-5253, Martin Co.

9 KUMMER, D. L. et al, "Shielded Composite Structures," AFML-TR-65-331, October 1965.

10 KINGERY, W. D., "Ceramic Fabrication Processes," The Technology Press of MIT and John Wiley & Sons, Inc., 1958.

11 DUCKWORTH, W., Journal of American Ceramic Society 36; 68 (1953).

REFERENCES (CONT)

12 SCHOFIELD, H. S.; LYNCH, J. E.; DUCKWORTH, D. W., "Fundamental Studies of Ceramic Material," Final Summary Report, Battelle Memorial Institute, Office of Naval Research, Navy Dept., Contract No. N5-ORI-111, March 31, 1949.

13 GAMON, R. E.; HARRIS, G. M.; VASILOS, T., "Effect of Porosity on Mechanical, Thermal and Dielectric Properties of Fused Silica," American Ceramic Bulletins, May 1965.

14 SPRIGGS, R. M., "Expression for Effect of Porosity on Elastic Modulus of Polycrystalline Refractory Materials, Particularly Aluminum Oxide," Journal of the American Ceramic Society 44, 628 (1961).

15 KNUDSEN, F. P., "Effect of Porosity on Young's Modulus," Journal of the American Ceramic Society 45, 94 (1962).

16 GALLAGHER, R. H.; PADLOG, J., BIJLAARD, "Stress Analysis of Heated Complex Shapes," American Rocket Society Journal, pp 700-707, May 1962.

17 "Investigation of Feasibility of Utilizing Available Heat Resistant Materials for Hypersonic Leading Edge Applications," WADC TR59-744, July 1960.

APPENDIX A

BASIS OF DETERMINING MATERIAL MECHANICAL AND THERMAL PROPERTIES

Literature data were utilized in establishing thermal and mechanical properties of the materials. Since test information is comparatively scarce for high-porosity ceramics, it is generally necessary to interpolate between test points or apply empirical or analytical relationships to approximate properties at porosities of interest.

1. Thermal Conductance

Thermal conductivity in high temperature porous structures was determined by the following expressions, based on the derivations of Reference 9:

$$\text{overall } k = k \text{ (conduction)} + k \text{ (radiation)}$$

$$k \text{ radiation} = 12\ d/2\ \sigma\epsilon/2\ T^3\ (p)$$

where p = porosity

d = spherical pore diameter

While k (conduction) is often taken to vary directly with (1-p), most experimental data show a sharper reduction in conductivity due to porosity. The (1-p) variation applies to an isolated pore geometry, and in general, compositions have some interconnection of pores.

Figure A-1 illustrates the effects of various types of porosity on thermal conductivity. As shown, a dashed line was arbitrarily selected as being representative of the porous materials.

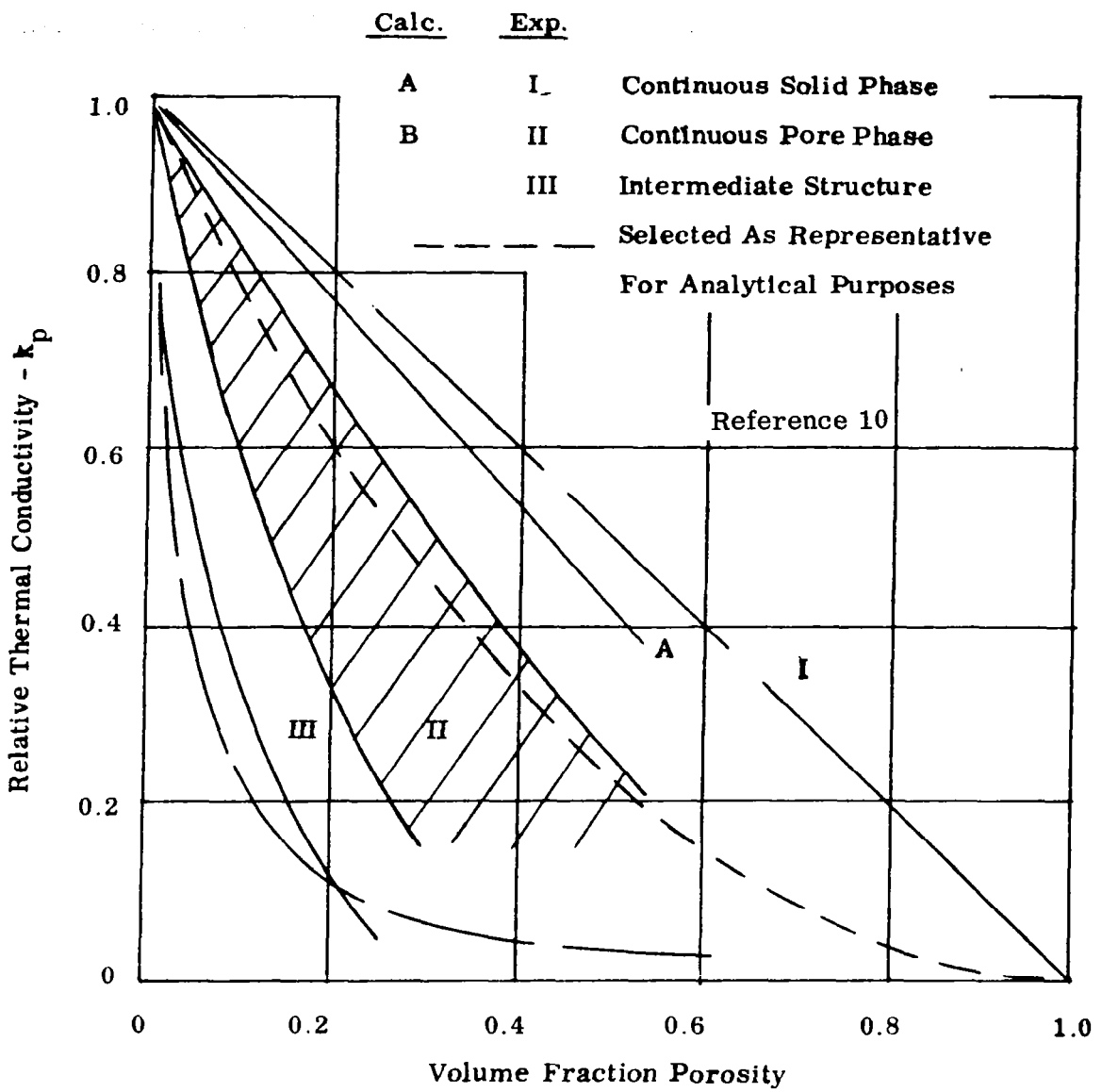

Figure A-1. Effects of Type and Amount of Porosity on Relative Conductivity

2. Effect of Porosity on Strength of Polycrystalline Ceramic Materials

The most commonly used relationships between strength and porosity are in the form:

$$\sigma = \sigma_o e^{-np} \qquad \text{(A-1)}$$

where σ_o is the strength of nonporous polycrystalline material and p is the volume fraction porosity.

Exponent n varies from four to seven and is characteristic of the material and the particular pore structure. Equation (A-1) applies well to low values of porosity (References 11, 12), but there are examples of good fit with experimental points also at high porosities. Reference 13 provides data which can be represented in the form of Equation (A-1) for fused silica to porosities of 80%. Reference 12 shows that n is equal to 5.21 for a particular low porosity alumina.

3. Effect of Porosity on the Elastic Modulus of Polycrystalline Ceramic Materials

An exponential form of the porosity-modulus relationship is given in Reference 14.

$$E = E_o e^{-k p}$$

Experimental k values are:

k = 6.6 for fused silica (Reference 13)

k = 2.4 to 4.4 for alumina with an average of 4.0 (References 14, 15)

APPENDIX B

THERMAL STRESS ANALYSIS METHODS

This appendix describes the thermal stress analysis used to calculate thermal stresses in the candidate ceramic materials.

1. Assumptions

   (a) Thermal gradients exist only in the direction normal to the plate. The heat input is an arbitrary function of time.

   (b) A straight line normal to the surface of the plate before heating remains a straight line after heating.

   (c) Only in-plane stresses are considered in the plate.

   (d) Shear stresses are neglected.

   (e) The plate may be restrained or unrestrained. In the solutions performed, the plate was considered completely unrestrained since it is intended to provide attachments which offer minimum restraints.

   (f) Adiabatic back-face conditions are assumed.

   (g) Temperature and porosity effects on material properties are considered.

2. Evaluation of Assumptions

The application essentially involves thermal gradients in one direction and in-plane thermal gradients are expected to be very small. More complex solutions using matrix methods for similar plate problems have shown that stresses normal to the plane and to the shear stresses are about zero except at the edges of the plate.

3. Elastic Analysis of a Composite Plate

The general expression for the thermal stress at any point j in the plate thickness is given by:

$$\sigma_{x_j} = \sigma_{y_j} = \left\{ - \alpha_j \Delta T_j + A \left[\frac{\int \alpha \Delta T \frac{E}{1-\upsilon} dz}{\int \frac{E}{1-\upsilon} dz} \right] + B z'_j \left[\frac{\int \alpha \Delta T z' \frac{E}{1-\upsilon} dz}{\int (z')^2 \frac{E}{1-\upsilon} dz} \right] \right\} \frac{E_j}{1-\upsilon_j} \qquad \text{(C-1)}$$

where ΔT equals the temperature changes and z' is the distance from the plate's neutral axis. The integrals in Equation (B-1) are integrated over the thickness of the plate from z = 0 to z = $(d_1 + d_2 + d_3)$, and α, ΔT, E, υ, and z' all vary with the thickness ordinate, z. Also, α, E, are temperature dependent.

The three terms within the brackets on the right-hand side of Equation (B-1) represent strains and each has a particular significance. The first term represents the full thermal strain corresponding to a completely fixed plate. The second term gives the in-plane strain relief if the plate is allowed to expand or contract. The second term is the full expansion of the plate provided by a complete freedom to expand. The third term is the strain relief provided by the bowing of the plate. The factor within the brackets is the reciprocal of the radius of curvature for a plate completely unrestrained against bowing.

In view of the importance of the bracketed factors in the second and third terms, it is convenient to express Equation (B-1) as:

$$\sigma_{x_j} = \sigma_{y_j} = \left\{ - (\alpha \Delta T)_j + A \epsilon + B_{z'_j} \omega \right\} \frac{E_j}{1-\nu_j} \qquad \text{(C-2)}$$

The evaluation of plate expansion ϵ and bowing ω are accomplished by numerical intergration and are discussed in the following paragraphs.

Factors A and B are support flexibility factors for expansion and bowing restraints, respectively. Either factor may be made equal to zero if the support conditions completely restrain the plate against the associated deformation, or may be made equal to unity if the plate is completely free.

4. Calculation of Plate Expansion

The free thermal expansion of the composite plate is determined by a numerical integration over the thickness of the plate from sublayer 1 to sublayer M (see Figure B-1) according to the following expression:

$$\epsilon = \frac{\sum_{j=1}^{j=M} \alpha_j \Delta T_j \left(\frac{E_j}{1-\nu_i} \right) \Delta z_i}{\sum_{j=1}^{j=M} \frac{E_j}{1-\nu_i} \Delta z_i} \qquad \text{(C-3)}$$

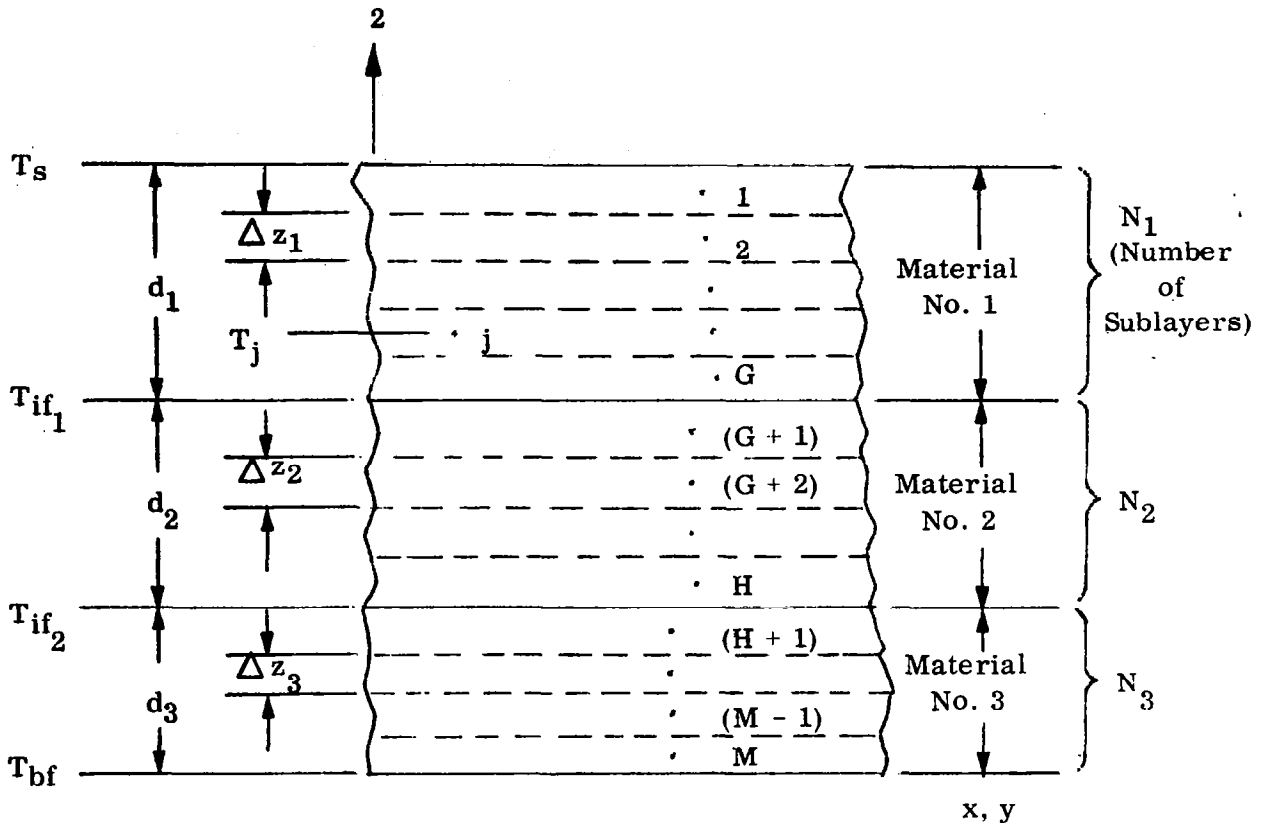

$$\Delta z_1 = \frac{d_1}{N_1} \qquad G = N_1$$

$$\Delta z_2 = \frac{d_2}{N_2} \qquad H = N_1 + N_2$$

$$\Delta z_3 = \frac{d_3}{N_3} \qquad M = N_1 + N_2 + N_3$$

Figure B-1. Geometry of Plate Cross-Section

where

i = 1 for j = 1, 2, 3,---G
i = 2 for j = G + 1,----H
i = 3 for j = H + 1,----M

$$\Delta T_j = T_j - T_o$$

The thermal expansion, α_j, and elastic modulus, E_j are evaluated at temperature T_j

5. CALCULATION OF NEUTRAL AXIS

In considering the thermal bowing of the plate, it is necessary to determine the location ($\bar{Z}$) of the neutral axis of the plate. The z coordinate to the center of each sublayer is given by:

$$z_1 = (d_1 + d_2 + d_3) - \frac{1}{2}\Delta z_1$$

$$z_j = z_1 - (j - 1)\Delta z_1 \text{ for } j = 2, 3, ---G$$

$$z_{(G+1)} = (d_2 + d_3) - \frac{1}{2}\Delta z_2 \qquad \textbf{B-4}$$

$$z_j = z_{G+1} - (j - G - 1)\Delta z_2 \text{ for } j = (G + 2),---H$$

$$z_{(H+1)} = d_3 - \frac{1}{2}\Delta z_3 \text{ (If } N_3 = 1 \text{ } (H + 1) = M)$$

$$z_j = z_{(H+1)} - (j - H - 1)\Delta z_3 \text{ for } j = (H + 2)---M$$

The location of the neutral axis is given by:

$$\bar{z} = \frac{\sum_{j=1}^{j=M} z_j \frac{E_j}{1-\nu_i}\Delta z_i}{\sum_{j=1}^{j=M} \frac{E_j}{1-\nu_i}\Delta z_i} \qquad \textbf{B-5}$$

From $\bar{z}$, the distance from the neutral axis to the center of each sublayer is:

$$z'_j = z_j - \bar{z} \qquad j = 1, 2, 3,----M \qquad \textbf{B-6}$$

6. CALCULATION OF THERMAL BOWING

The free thermal bowing of the plate is determined by numerical integration over the thickness increments of the plate. The curvature (reciprocal of the radius of curvature) of the plate is given by:

$$\omega = \frac{\sum_{j=1}^{j=M} \alpha_j \, \Delta T_j \, z'_j \frac{E_j}{1-\nu_i} \Delta z_i}{\sum_{j=1}^{j=M} \left(z'_j\right)^2 \frac{E_j}{1-\nu_i} \Delta z_i} \quad (\text{in.}^{-1}) \qquad \text{B-7}$$

7. DETERMINATION OF THERMAL STRESSES

The thermal stresses are determined at the upper and lower boundaries of each of the three materials regardless of the support conditions. In addition, if the plate is free to bow (i.e., B = 1.0), the stresses are calculated for each sub-layer.

The set of six boundary stresses is given by:

$$\sigma_{x_{1U}} = \left[-\alpha_{1U}(T_s - T_o) + A\epsilon + B\,(d_1 + d_2 + d_3 - \bar{z})\,\omega \right] \frac{E_{1U}}{1-\nu_1}$$

$$\sigma_{x_{1L}} = \left[-\alpha_{1L}(T_{if_1} - T_o) + A\epsilon + B\,(d_2 + d_3 - \bar{z})\,\omega \right] \frac{E_{1L}}{1-\nu_1}$$

$$\sigma_{x_{2U}} = \left[-\alpha_{2U}(T_{if_1} - T_o) + A\epsilon + B\,(d_2 + d_3 - \bar{z})\,\omega \right] \frac{E_{2U}}{1-\nu_2} \qquad \text{(B-8)}$$

$$\sigma_{x_{2L}} = \left[-\alpha_{2L}(T_{if_2} - T_o) + A\epsilon + B\,(d_3 - \bar{z})\,\omega \right] \frac{E_{2L}}{1-\nu_2}$$

$$\sigma_{x_{3U}} = \left[-\alpha_{3U}(T_{if_2} - T_o) + A\epsilon + B\,(d_3 - \bar{z})\,\omega \right] \frac{E_{3U}}{1-\nu_3}$$

$$\sigma_{x_{3L}} = \left[-\alpha_{3L} (T_{bf} - T_o) + A\epsilon - B\bar{z}) \omega \right] \frac{E_{3L}}{1-\upsilon_3}$$

The thermal expansion, α_k, and elasticity, E_k, are evaluated at temperature, T_k.

The sublayer stresses are assumed to act at the center of the sublayer and are expressed by:

$$\sigma_{x_j} = \sigma_{y_j} = \left[-\alpha_j \Delta T_j + A\epsilon + B z_j \omega \right] \frac{E_j}{1-\upsilon_i} \qquad \text{(B-9)}$$

Where j 1, 2, 3 ----------M

8. TEMPERATURE ANALYSIS

Since no temperature gradients in the plane of the plate are considered, the heat flow is one dimensional, flowing only in the direction normal to the surfaces of the plate. The temperature analysis of the composite plate is a transient solution utilizing a finite difference technique to solve the heat conduction through the plate. The method consists in dividing time into small increments, Δ t, and the plate thickness into small increments, Δ z. By means of heat balances for each of the space increments (Δ z's), the finite difference solution proceeds from one time increment to the next in the following manner. From the temperatures existing at the beginning of a time interval the change in temperature of each thickness increment, which occurs during the time interval under consideration, is calculated. By adding these changes to the temperatures at the beginning of the time interval a set of new temperatures is obtained corresponding to the end of the time interval. These new temperatures then become the starting conditions in the next time interval and the calculation process is repeated. The variations in thermal properties with temperature are considered.

Since this approach is fairly well known, the thermal analysis method will not be described in further detail.

APPENDIX C

TYPICAL THERMAL STRESS ANALYSIS RESULTS

This appendix presents the results of the thermal stress studies for an alumina module 1/2 inch (12.7 mm) tnick, with a 0.015 inch (0.381 mm) pore diameter, and 50 lb/ft^3 (799 kg/m^3) in density. The analysis is based on the first four minutes of the abort trajectory for a vehicle surface 2 feet (0.609 m) from the nose on the lower body centerline.

Similar analyses for other materials studied are presented in Reference 1.

TABLE C-1

THERMAL PROPERTIES OF ALUMINA

100% Dense = 248 lb/ft^3, 3960 kg/m^3

Surface Emissivity = 0.55 (Cr_2O_3 - coated) Reference 9

Emissivity of Al_2O_3 = 0.3

Specific Heat				Thermal Expansion		
Reference 7				Reference 9		
Temp. °F	°K	BTU/lb - °F	J/kg - °K	Temp °F	°K	%
0	255	0.20	840	0	255	0
250	394	0.228	960	1000	811	0.40
500	533	0.250	1050	2000	1365	0.84
750	671	0.262	1100	3000	1922	1.32
1000	811	0.275	1155			
1500	1090	0.280	1175			
2000	1365	0.29	1220			
2500	1645	0.30	1260			
3000	1922	0.32	1340			
3500	2200	0.34	1430			

NOTE: The specific heat and thermal expansion are assumed to be independent of the density. The specific heat was extrapolated linearly beyond 2700°F (1756°K).

TABLE C-2

CALCULATED THERMAL CONDUCTANCE FOR ALUMINA

Emissivity = 0.3

Average Pore Diameter = 0.015 inch, 0.00038 m

Theoretical Density = 248 lb/ft^3, 3960 kg/m^3

	Thermal Conductivity in BTU-in./hr.ft^2-°F, (J/m-sec-°K)				
Porosity	0	0.20	0.40	0.60	0.80
Temp.	(a) 250(36)	150(21.6)	82.5(11.2)	37.5(5.4)	9.9 (1.4)
60°F	(b) 0 (0)	0 (0)	0 (0)	0 (0)	0 (0)
288°K	(c) 250(36)	150(21.6)	82.5(11.2)	37.5(5.4)	9.9 (1.4)
250°F	200(29)	120(17.3)	66 (9.5)	30 (4.3)	8.0 (1.15)
	0 (0)	0 (0)	0 (0)	0 (0)	0 (0)
394°K	200(29)	120(17.3)	66 (9.5)	30 (4.3)	8.0 (1.15)
500°F	140(20)	84(12.1)	46.2(6.6)	21 (3.0)	5.6 (0.80)
	0 (0)	0 (0)	0 (0)	0 (0)	0 (0)
533°K	140(20)	84(12.1)	46.2(6.6)	21 (3.0)	5.6 (0.80)
750°F	105(15)	63 (9.1)	34.6(5.0)	15.8(2.3)	4.75(0.58)
	0 (0)	0 (0)	0 (0)	0 (0)	0 (0)
672°K	105(15)	63 (9.1)	34.6(5.0)	15.8(2.3)	4.75(0.58)
1000°F	80(11.5)	48 (6.9)	26.4(3.8)	12.0(1.7)	3.25(0.47)
	0 (0)	0 (0)	0 (0)	0 (0)	0.1 (0)
811°K	80(11.5)	48 (6.9)	26.4(3.8)	12.0(1.7)	3.35(0.47)
1500°F	55(7.9)	33 (4.8)	18.2(2.6)	8.4(1.2)	2.34(0.34)
	0 (0)	0 (0)	0 (0)	0.1 (0)	0.1 (0)
1090°K	55(7.9)	33 (4.8)	18.2(2.6)	8.5(1.2)	2.44(0.34)
2000°F	45(6.5)	27 (3.9)	15.0(2.1)	7.0(1.0)	2.1 (0.30)
	0 (0)	0 (0)	0.1 (0)	0.2 (0)	0.3 (0.04)
1365°K	45(6.5)	27 (3.9)	15.1(2.1)	7.2(1.0)	2.40(0.34)
2500°F	40(5.8)	24 (3.5)	13.4(1.9)	6.4(0.9)	2.1 (0.30)
	0 (0)	0.1 (0)	0.2 (0)	0.4(.06)	0.5 (.07)
1645°K	40(5.8)	24.1(3.5)	13.6(1.9)	6.8(0.96)	2.6 (0.37)
3000°F	40(5.8)	24 (3.5)	13.6(1.96)	6.6(.95)	2.4 (0.35)
	0 (0)	0.2 (0)	0.4(.06)	0.6(.09)	0.8 (.11)
1922°K	40(5.8)	24.2(3.5)	14.0(2.02)	7.2(1.04)	3.2(0.46)
3500°F	40(5.8)	24 (3.5)	13.8(1.99)	6.9(1.0)	2.8(0.40)
	0 (0)	0.3(.04)	0.6(.09)	0.9(.13)	1.2(0.17)
2200°K	40(5.8)	24.3(3.54)	14.4(2.08)	7.8(1.13)	4.0(0.57)

Legend:
(a) Conductance component through solid material, k_c (refer to Appendix A).
(b) Radiation component across pores, k_r (refer to Appendix A).
(c) Total thermal conductivity, $k_c + k_r$

TABLE C-3

MECHANICAL PROPERTIES OF ALUMINA

Porosity		Modulus of Elasticity (Note 1), 10^6 lb/in^2(10^9 kg/m^2)			
		0.02	0.20	0.60	0.80
Temp. °F	°K				
80	300	57.5(40.2)	25.5(17.9)	5.2(3.6)	2.3(1.6)
500	533	55.3(38.7)	24.5(17.1)	5.0(3.5)	2.3(1.6)
1000	811	53.7(37.6)	23.8(16.6)	4.9(3.4)	2.2(1.5)
1500	1090	50.0(35.0)	22.2(15.5)	4.5(3.1)	2.0(1.4)
1830	1270	48.0(33.6)	21.3(14.9)	4.4(3.1)	2.0(1.4)
2170	1405	41.7(29.2)	18.5(12.9)	3.8(2.7)	1.7(1.2)
2500	1645	32.3(22.6)	14.3(10.0)	2.9(2.0)	1.3(0.9)
2770	1795	22.9(16.0)	10.1(7.1)	2.1(1.5)	0.9(0.63)
3000	1922	13.0(9.1)	5.8(4.1)	1.2(.85)	0.5(0.35)
3300	2090	0 (0)	0 (0)	0 (0)	0 (0)

NOTE 1: The modulus of elasticity vs temperature for 98% dense are from Reference 7. The variation with porosity is assumed to conform to the relation $E = E_o e^{-4P}$. Values above 2700°F (1755°K) were assumed to approach zero linearly.

TABLE C-3 (CONT)

MECHANICAL PROPERTIES OF ALUMINA

		Tensile Strength (Note 2)			
Porosity		0.02	0.20	0.40	0.50
Temp. °F	°K	10^3 lb/in^2 (10^6 kg/m^2)			
70	294	37.5(26.2)	14.0(9.8)	6.98(4.9)	5.36(3.75)
1200	922	36.0(25.2)	13.4(9.4)	6.70(4.7)	5.15(3.6)
1500	1090	35.0(24.5)	13.0(9.1)	6.51(4.5)	5.00(3.5)
1600	1045	33.7(23.6)	12.5(8.8)	6.26(4.4)	4.82(3.4)
1750	1228	31.2(21.8)	11.6(8.1)	5.80(4.1)	4.46(3.1)
1900	1311	27.5(19.2)	10.2(7.1)	5.11(3.6)	3.93(2.8)
2440	1610	12.0(8.40)	4.46(3.1)	2.23(1.6)	1.72(1.2)
2550	1670	6.0(4.20)	2.23(1.6)	1.12(7.8)	0.86(0.60)
3000	1922	2.5(1.75)	0.93(0.65)	0.47(0.33)	0.36(0.25)
3300	2090	0 (0)	0 (0)	0 (0)	0 (0)

NOTE 2: The variation with density conforms to Reference 7 except that $\sigma = \sigma_o e^{-4P}$ was assumed for porosities above 50%.

TABLE C-3 (CONT)

MECHANICAL PROPERTIES OF ALUMINA

		Compressive Strength (Note 3)			
Porosity		0.02	0.20	0.40	0.50
Temp. °F	°K	10^3 lb/in^2, (10^6 kg/m^2)			
0	255	320(224)	76.8(54)	21.6(15)	18.0(13)
500	533	225(158)	54.0(38)	19.9(14)	12.7(8.9)
1000	811	160(112)	38.4(27)	11.6(8.1)	9.0(6.3)
1500	1090	120(84)	28.8(20)	8.5(5.9)	6.8(4.8)
2000	1365	70(49)	16.8(12)	4.9(3.4)	3.9(2.7)
2500	1645	30(21)	7.2(5)	2.1(1.5)	1.7(1.2)
3000	1922	6(4)	1.4(1)	0.4(0.3)	0.3(0.2)
3300	2090	0(0)	0(0)	0(0)	0(0)

NOTE 3: The compressive strength for 100% dense and variation with density are from Reference 7, except that $\sigma = \sigma_o e^{-4P}$ was assumed for porosities above 50%.

TABLE C-4

MAXIMUM STRESS CONDITIONS

Time Seconds	Distance From Outer Surface		Temperature		Stress		$\left(\frac{\sigma}{\sigma_A}\right)$
	Inches	mm	°F	°K	lb/m^2	$10^3 kg/m^2$	
113.6	0.0	0	2975	1908	-2961	-2070	-16.685
	0.033	0.84	2557	1676	-4508	-3160	- 6.701
	0.100	2.54	1698	1199	- 393	- 275	- 0.158
	0.166	4.22	1204	924	2863	2000	1.265
	0.200	5.08	1053	840	3403	2380	1.500
	0.233	5.82	933	774	3506	2450	1.536
	0.300	7.62	783	690	2437	1705	1.063
	0.366	9.30	695	641	455	318	0.197
	0.400	10.28	671	628	- 826	- 578	- 0.164
	0.425	10.80	653	618	-1799	-1259	- 0.354
	0.475	12.08	636	609	-4015	-2802	- 0.783
	0.500	12.70	627	604	-5125	-3585	- 0.994
133.2	0.0	0	3025	1936	-1571	-1100	-11.541
	0.033	0.84	2796	1809	-2463	-1722	- 6.325
	0.100	2.54	2159	1455	-1358	- 951	- 0.959
	0.166	4.22	1631	1161	1470	1030	0.7
	0.200	5.08	1437	1054	2323	1625	1.049
	0.266	6.75	1279	966	2799	1958	1.249
	0.300	7.62	1064	847	2448	1715	1.077
	0.366	9.30	938	777	829	580	0.363
	0.400	10.28	904	752	- 402	- 281	- 0.0894
	0.425	10.80	881	744	-1356	- 950	- 0.313
	0.475	12.08	859	733	-3611	-2525	- 0.820
	0.500	12.70	847	726	-4741	-3315	- 1.068

$\frac{\sigma}{\sigma_A}$ is the ratio of stress to allowable stress.
Negative numbers denote compression stress.
Positive numbers denote tensile stress.

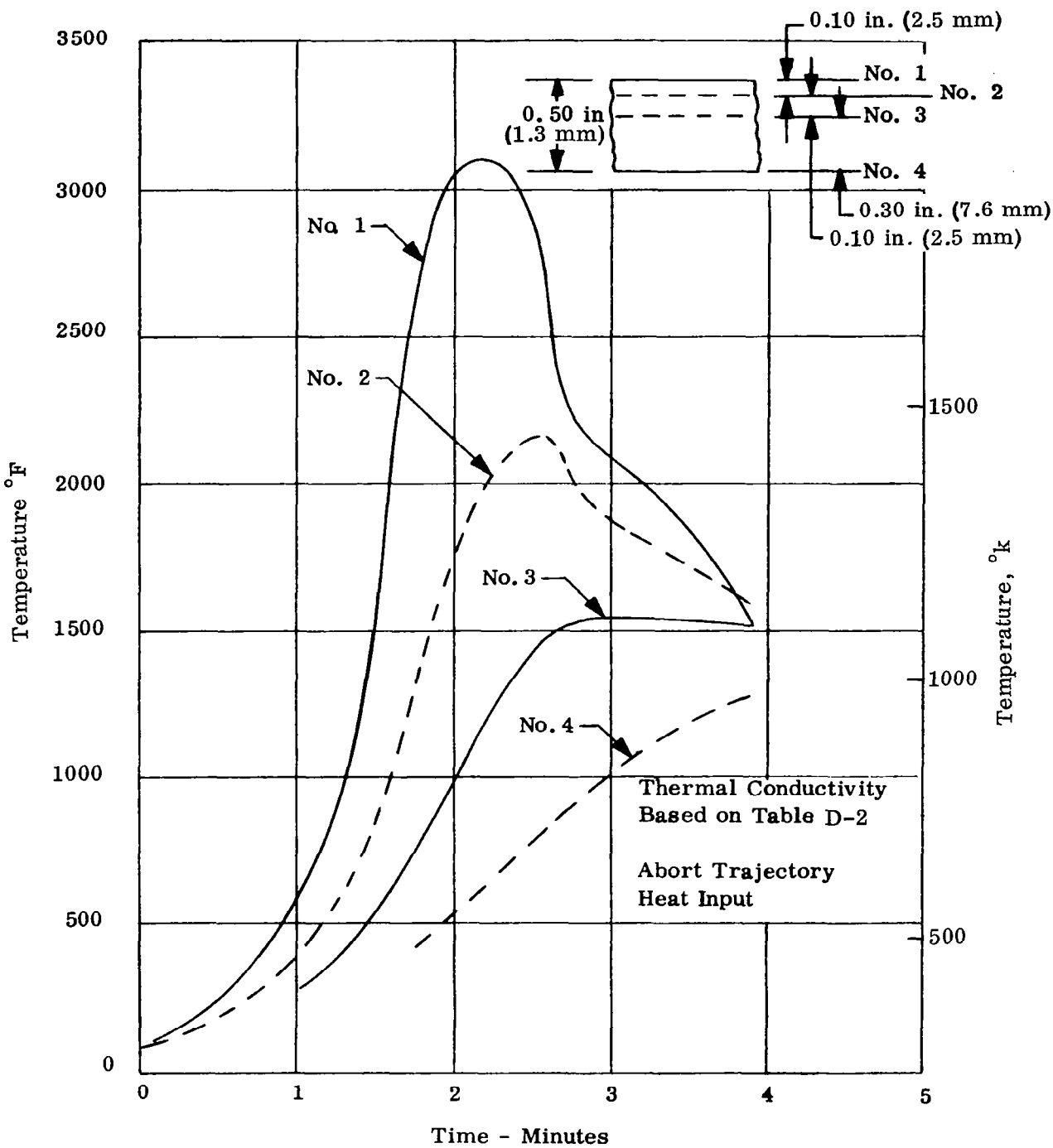

Figure C-1. Thermal Analysis of 50 lb/ft^3 (799 kg/m^3) Alumina with 0.015 in. (0.00038 m) Pore Diameter

APPENDIX D

ATTACHMENT DESIGN

1. Analysis of Interface Stresses

To determine the feasibility of thin metal attachments to ceramic bodies, a matrix thermal stress analysis (Reference 16) was performed to determine the stresses in a 3 x 3 x 1/2 inch (0.76 x 0.76 x 0.0127 m) zirconia plate and a columbium (F-48) metal foil 0.003 inch (7.6 mm) thick which were rigidly bonded and heated from 0 to 2000°F (1365°K). The mean thermal expansion coefficients of zirconia were higher than those of columbium by 1.4×10^{6} inch/inch - °F (2.5×10^{6} m/m - °K) at low temperatures and 0.5×10^{-6} inch/inch - °F (0.9×10^{-6} m/m - °K) at the maximum temperature. Figure D-1 shows that the stresses in the ceramic are limited to 666 psi (466×10^{3} kg/m^2) compression, while the foil stresses are 15,394 psi (10.76×10^{6} kg/m^2) tension. Also, the stresses in the ceramic decrease rapidly with distance from the foil.

The example illustrates the principle of using thin metal attachments to limit ceramic stresses. Since the ceramic stresses are characteristically localized at the interface vicinity, the ceramic may be densified in this area to meet strength requirements without adding substantial weight. In this example, the densified zone would be expected to be 0.05 inch (1.27 mm) thick, judging from the stress distribution of Figure D-1.

2. Stresses Due to Thermal Expansion Characteristics of Feltmetal and Ceramics

The feltmetal interlayer between the ceramic module and the support structure will be approximately 10% dense and will have an extremely low modulus of elasticity. Any stresses that will develop from the thermal expansion differences will be localized where the feltmetal fiber is embedded in ceramic or ceramic adhesive. A simple analysis follows:

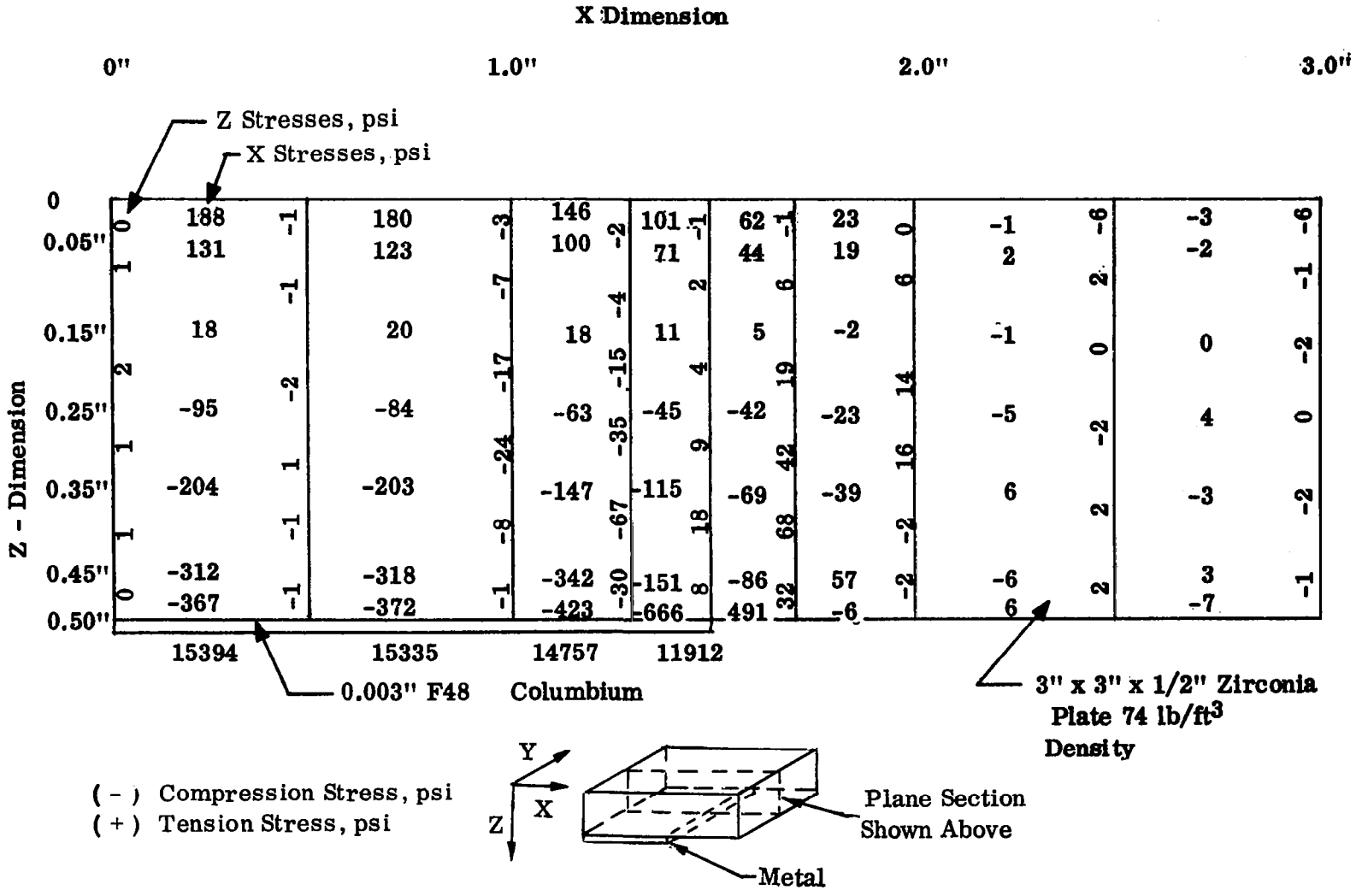

Figure D-1. XZ Stresses in Ceramic-Metal System

a. Metal Wires Embedded in Ceramic

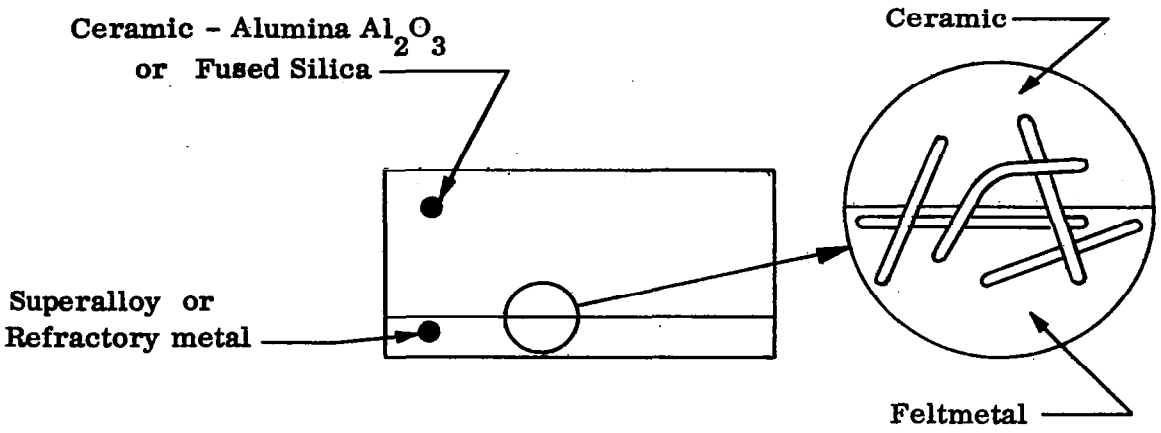

b. Tension and Compression Stresses in Ceramic and Metal

Referring to Figure D-1, it is seen that only the ceramic layer immediately adjacent to the interface is highly stressed. This layer is approximately 0.050 inch (1.27 mm) thick, as judged from the stress distributions. Therefore, assuming that all the stress arising from the joint will be concentrated in this layer, the following expressions are developed:

A_c, Stressed Ceramic Section = $\pi r_c^2 - \pi r_w^2$

where r_c = 0.0050 inch (1.27 mm) and is the radius of the stressed ceramic section and r_w is the wire radius.

$P = \epsilon E_w A_w = \epsilon E_w \pi r_w^2$,

where P is the total force per unit length generated by the restraint of the wire corresponding to a strain ϵ

σ_{cer}, Stress in Ceramic = $P/A = \pi r_c^2 - \pi r_w^2 / \epsilon E \pi r_w^2$

σ_w, Stress in Wire = ϵE_w

c. Shear Stresses

$P = \epsilon A_W E_W$ for unit length

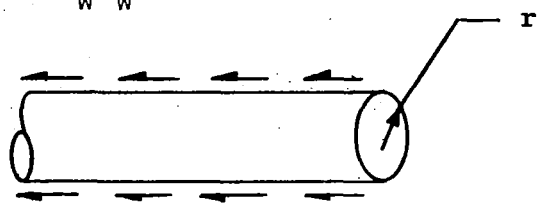

cross-sectional area $A = \pi r^2$

Shear area, circumferential area $A_s = 2\ \pi rL(L = 1)$

$P = \epsilon \pi r^2\ E_W$

If load is transferred as shear only, assuming constant shear stresses:

$$\sigma_s = P/A_s = \frac{\epsilon\ \pi\ r_W^2}{2\ \pi r_W} = \frac{\epsilon\ r_W\ E_W}{2}$$

The results of an analysis is based on the indicated relationships are presented in Table IX. The Cb alloy-alumina and the Ta alloy-alumina combinations are particularly attractive since acceptable alumina metal and shear stresses result.

3. Removal and Installation of Heat Shield Panels When Interior Access is not Available

It is extremely desirable to have the capability to remove and install heat shield panels when access to vehicle interior is difficult as in the case of replacing a damaged panel on a completed vehicle. In general, the attachment design can be developed according to the following requirements:

a. Weight to be equal to or less than a conventional screw and nut.

b. Individual panels to be installed and removed without access to interior of vehicle.

c. Attachment must not create unacceptable restraint to the thermal expansion of the panel support.

d. Where silicone elastomeric materials are used, the maximum short time temperature should not exceed 500 °F (533 °K).

One approach, which is simple mechanically but requires a satisfactory ceramic adhesive, is to provide access holes in the ceramic and metal panel and suitable plugs. In this event, a 1/4 inch (0.0063 m) diameter hole is fabricated into the metallic panel directly over each attachment hole in the support leg. A 1/2 inch (0.0127 m) diameter hole concentric with the 1/4 inch (0.0063 m) diameter hole is cored out in the ceramic foam and feltmetal laminate during the fabrication operation.

For panel attachment to the primary structure, stainless steel socket-heat screws and floating nut plates are used. Access to these is via the panel holes using a hexagonal tip screw driver. After panel assembly, the 1/2 inch (0.0127 m) diameter hole in the ceramic is plugged with a slightly smaller slug of the same material using ceramic bonding cement. This method is shown in the configuration drawing of Figure D-2.

Figure D-3 shows a typical mechanical type latch; the principle of operation is evident by visual inspection. Removal of this panel requires core-drilling a hole through the panel construction immediately above the stud which is welded into the support leg. Using a piloted end mill in a hand drill, the welded area about the stud is milled off releasing the panel support legs. The stud is removed by turning it 90° to bring the plateau lands on the stud end into bearing on the spring clip ends forcing them apart. The stud may then be withdrawn. An additional item required with this type of attachment is a thin wall sleeve which slips over the stud to prevent engagement of stud retainer spring with stud grooves during prefitting and panel height adjustments which may be required.

Figure D-4 is an example of a bonded elastomeric joint which takes advantage of the room temperature self-vulcanizing properties of several two-part silicone rubber compounds which are applied in a semi-liquid or paste-like condition. The cured materials exhibit excellent adhesion to clean, etched metallic surfaces with very little shrinkage and can withstand temperatures of 500 to 600 °F (533 - 590 °K) for short times (approximately 10 minutes) without serious deterioration. The joint shown resists tensile loads by shear in the rubber which completely fills the retainer cup.

Note that there is an additional locking device (elliptic spring ring in stud groove) which is designed to prevent pullout of the stud in the event of shear or bond failure in the elastomer. Necessary panel height adjustment is accomplished by shimming under stud retainer cup. Thus, the support leg stud enters the retainer cup a fixed distance and engagement of the lock ring is always assured. The mounting also has an additional feature in that the top plate of the stud retainer cup is fabricated of high conductivity aluminum and the stud materials is a low conductivity superalloy. This minimizes heat conduction into the silicone elastomer.

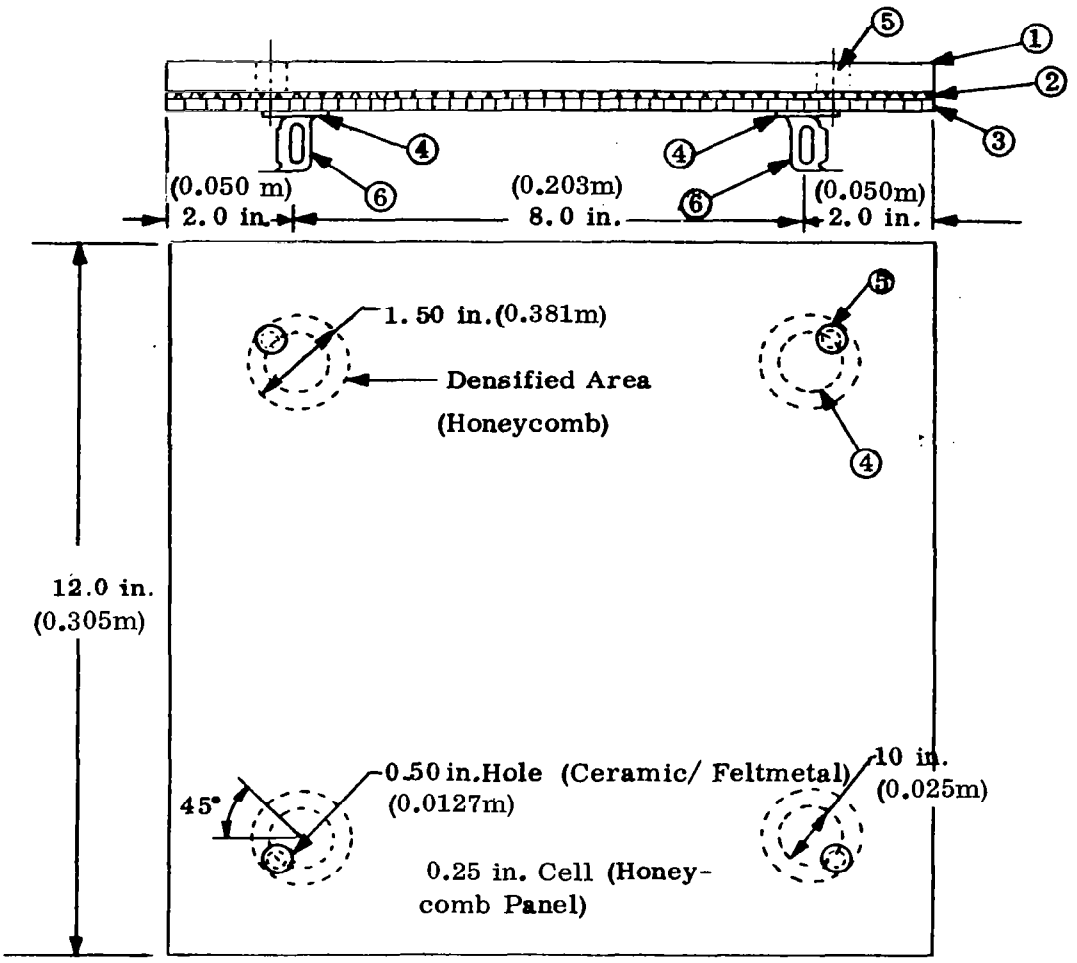

Notes:

1. Alumina foam ceramic.
2. 10% density feltmetal.
3. Honeycomb sandwich - Hastelloy X.
4. Support reinforcing pad brazed to panel.
5. Cemented foam ceramic plug.
6. Support leg attached to drilled Support pad, using two 3/32 in. (0.0024m) in. diameter blind rivets. Assume rivet clamping force is 125 lb. (56.7 kg) per rivet.

Figure D-2. Panel with Plugged Mounting Access Holes

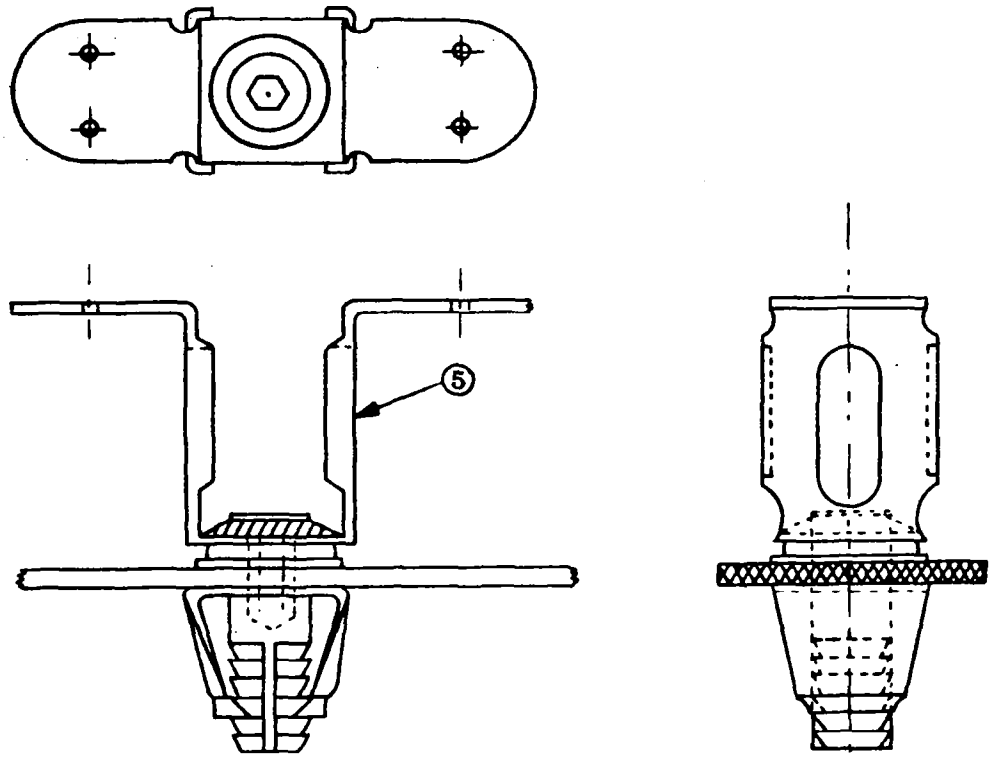

View I

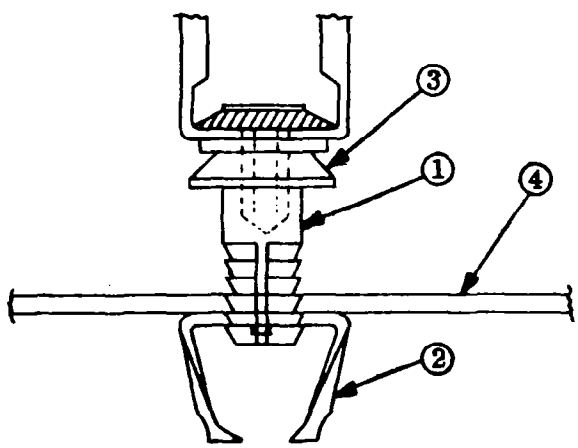

View II

Notes:

1. Hollow ratchet stud (flare or weld to attach to support leg) with internal hexagonal recess.
2. Spring clip stud retainer.
3. Bellville spring washer (Compressed)
4. Primary structure skin.
5. Panel support leg.

View I - welded stud in locked position.
View II - welded stud in unlocked position.

Figure D-3. Blind - Mechanical Latch Fasteners for Heat Shield

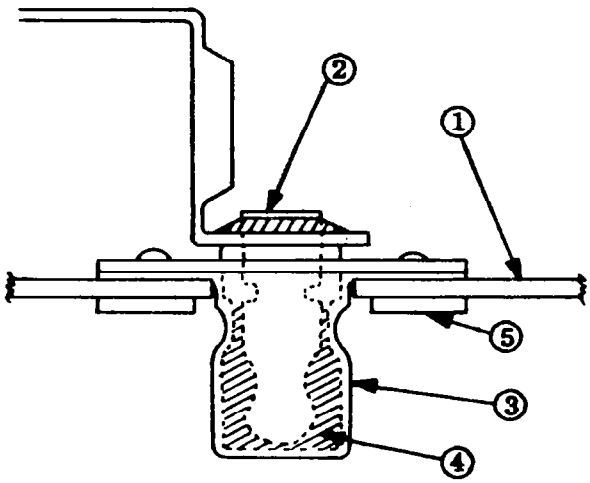

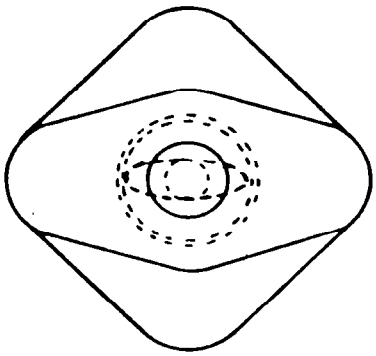

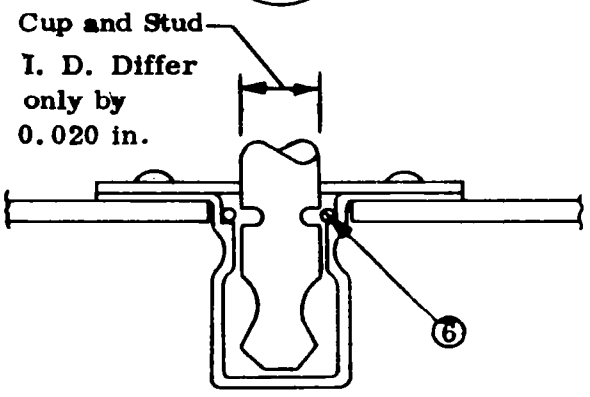

Notes:

1. Primary structure skin.
2. Support stud – low conductivity alloy.
3. Stud retainer cup – make from high conductivity alloy to form heat shunt.
4. R. T. curing silicone rubber.
5. Weld studs or thread inserts for cup attach screws.
6. Stud lock ring (elliptical).

To Install:

1. Panel is fitted dry to check level of panel with adjacent panels or installation gage. Shim as required to bring to proper level.
2. A metered amount of uncured silicone rubber paste is introduced into stud retainer cups and panel set in place, adjusted for position and weighted for 12 hours until silicone paste is cured.

To Remove:

1. Drill off flare from stud and remove panel.
2. Unscrew stud cup assembly and discard. Install new stud cup for new panel.

Figure D-4. Blind - Quick, Attach Fasteners for Heat Shield

APPENDIX E

ONE-DIMENSIONAL HEAT TRANSFER AND UNIT WEIGHT COMPUTATIONAL PROGRAM DESCRIPTION

This transient analysis procedure was utilized to determine temperature distributions through the heat shield components, including the ceramic module, insulation and support panels and to determine the trade-offs between insulation thickness and the cooling system requirements. The results of Figures 19 and 20 were obtained through this program.

The transient heat transfer analysis utilizes a finite difference solution. The method essentially divides time into small increments, $\Delta\theta$, and the thermally protected structural cross-section into small increments, ΔX, in the direction of the heat flow; i.e., normal to the plane of the outer surface. Utilizing heat balance equations for each of the space increments (ΔX's), the finite difference solution proceeds from one time increment to the next in the following manner.

From the temperatures existing at the beginning of a time interval, the changes in temperature of each space increment and the changes in the heat flows which occur during the time interval under consideration are calculated. By adding these changes to the values at the beginning of the time interval, a set of new temperatures and heat flows is obtained corresponding to the end of the time interval. These new temperatures and heat flows then become the starting conditions for the next time interval and the calculation process is repeated.

1. Description of Mathematical Model

The mathematical thermal model of the cross-section is given in Figure E-1. The mathematical model considers joint conductances at the interfaces of the insulation layers and the metallic sheets and at the connections between the intersheet supports. The joint conductances, h, are identified by double subscripts which designate the material bounding the joint.

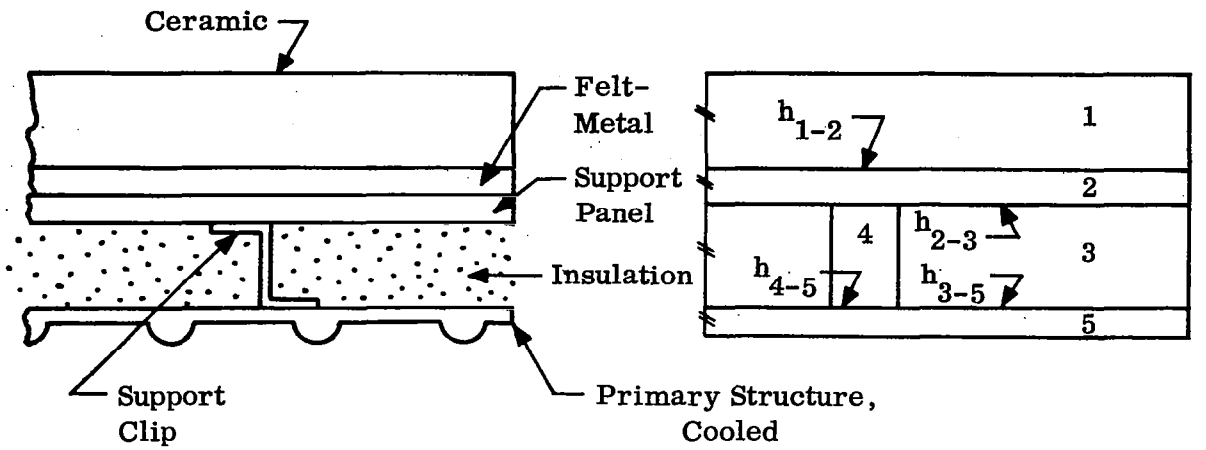

Idealized Elements

1. Ceramic Insulation
2. Metallic Sheet to Represent Support Panel and Feltmetal Heat Capacity
3. Lightweight Insulation
4. Metallic Heat Path Representative of the Support Clips
5. Metallic Sheet Representative of the Cooled Primary Structure

h_{1-2} Represents Thermal Conductance of Feltmetal

h_{2-3} Thermal Conductance of Interface Between Elements 2 and 3

h_{3-5} Thermal Conductance of Interface Between Elements 3 and 5

h_{4-5} Thermal Conductance of Interface Between Elements 4 and 5

Figure E-1. Mathematical Representation of the Heat Shield for Transient Thermal Analysis

The thicknesses of the insulation materials are divided into increments, ΔX. These have significant temperature gradients through their thicknesses and both the effects of heat capacity and thermal conductivity are considered.

The cooled metallic sheet, (5), is considered to have finite heat capacity and infinite thermal conductivity; i.e., at any given time the temperature through the sheet thickness is uniform. For the interwall support, (4), the heat capacity is assumed to be zero and the thermal conductivity finite. Element 2 represents the heat capacity of the support panel and feltmetal, while the thermal conductance of the two components is considered by the conductance h_{1-2}.

2. Material Properties

Input data for the program consisted of the following material properties; density, thermal conductivity, thickness, and specific heat. Specific heat and thermal conductivity may vary with temperature.

3. Heat Input

The heat input, which varies with flight time, is computed from the cold wall heat flux, $\dot{q}$, and the boundary layer recovery temperature, T_R. The heat input to the outer surface at any time is expressed by:

$$\dot{q}_1 = \dot{q} \left(\frac{T_R - T_1}{T_R - T_{w_o}} \right) - \epsilon_o \sigma (T_{1,})^4$$

where T_1 is the absolute surface temperature and T_{w_o} is the cold temperature from

$$\dot{q} = h_{b_1} (T_R - T_{w_o})$$

4. Cooling Options

The program provides for the cooling of the three metallic sheets by the specification of a maximum temperature for each sheet. When the temperature of a sheet rises to the maximum temperature, the temperature of the sheet remains at the maximum and the heat flow into the sheet is accumulated. The accumulated heat flow is used to determine the expended coolant required to cool the sheet.

5. Heat Flows

In order to examine the importance of the various heat paths, the heat flows (through the individual paths between the metallic sheets) are continually accumulated for the entire transient solution.

6. Selection of Space and Time Increments

To insure stability in the finite difference solution, the following relationship must be maintained between the thickness of the space increments (ΔX) for Materials (1), (3) and the time increments, $\Delta\theta$:

$$\Delta\theta \leq \frac{(\Delta X)^2}{2a}$$

where a = the thermal diffusivity of the material under consideration

NASA-Langley, 1967 —— 31 CR-861

"The aeronautical and space activities of the United States shall be conducted so as to contribute . . . to the expansion of human knowledge of phenomena in the atmosphere and space. The Administration shall provide for the widest practicable and appropriate dissemination of information concerning its activities and the results thereof."

—NATIONAL AERONAUTICS AND SPACE ACT OF 1958

NASA SCIENTIFIC AND TECHNICAL PUBLICATIONS

TECHNICAL REPORTS: Scientific and technical information considered important, complete, and a lasting contribution to existing knowledge.

TECHNICAL NOTES: Information less broad in scope but nevertheless of importance as a contribution to existing knowledge.

TECHNICAL MEMORANDUMS: Information receiving limited distribution because of preliminary data, security classification, or other reasons.

CONTRACTOR REPORTS: Scientific and technical information generated under a NASA contract or grant and considered an important contribution to existing knowledge.

TECHNICAL TRANSLATIONS: Information published in a foreign language considered to merit NASA distribution in English.

SPECIAL PUBLICATIONS: Information derived from or of value to NASA activities. Publications include conference proceedings, monographs, data compilations, handbooks, sourcebooks, and special bibliographies.

TECHNOLOGY UTILIZATION PUBLICATIONS: Information on technology used by NASA that may be of particular interest in commercial and other non-aerospace applications. Publications include Tech Briefs, Technology Utilization Reports and Notes, and Technology Surveys.

Details on the availability of these publications may be obtained from:

SCIENTIFIC AND TECHNICAL INFORMATION DIVISION

NATIONAL AERONAUTICS AND SPACE ADMINISTRATION

Washington, D.C. 20546